An Early Permian (ca. 280 Ma) silicic igneous province in the Alxa Block, NW China: A magmatic flare-up triggered by a mantle-plume?

CrossMark

Wei Dan [a,b,*], Xian-Hua Li [b], Qiang Wang [a,**], Gong-Jian Tang [a], Yu Liu [b]

[a] State Key Laboratory of Isotope Geochemistry, Guangzhou Institute of Geochemistry, Chinese Academy of Sciences, Guangzhou, Guangdong 510640, China
[b] State Key Laboratory of Lithospheric Evolution, Institute of Geology and Geophysics, Chinese Academy of Sciences, Beijing 100029, China

ARTICLE INFO

ABSTRACT

Silicic igneous provinces have important implications for geodynamic processes. In this study, we show that the predominantly Early Permian (ca. 280 Ma) granitoids in the Alxa Block correspond to an important silicic igneous province with areal distribution in Northwest (NW) China. We present zircon U–Pb age and Hf–O isotopic, and whole-rock geochemical and Sr–Nd isotopic data for the newly identified I- and A-type granites and high Sr/Y granodiorites in the Bayannuoergong batholith, and gabbros, diorites and quartz diorites in the Bijiertai Complex, Alxa Block. The I-type monzogranites, granodiorites and A-type granites of the Bayannuoergong batholith were probably generated by mixing between crust- and mantle-derived magmas, partial melting of a thickened eclogitic lower crust and underplated mantle-derived mafic rocks, respectively. The gabbros, quartz diorites and diorites of the Bijiertai Complex were likely generated by partial melting of the lithospheric mantle, differentiation from basaltic magmas and partial melting of the middle crust, respectively. Despite pronounced geochemical and isotopic heterogeneity of these rocks, new SIMS and LA–ICP-MS U–Pb zircon dating indicates that they were formed over a very short time interval at ca. 280 Ma. Thus, the mantle, lower crust and middle crust underwent widespread melting at this time. Given that these magmatic rocks have no spatial or temporal zonation, and were probably formed in an extensional setting, we suggest that the ca. 280 Ma Tarim mantle plume in NW China may have triggered the magmatic flare-up of the Alxa silicic igneous province.

© 2014 Elsevier B.V. All rights reserved.

1. Introduction

Silicic large igneous provinces (SLIP), composed of predominantly silicic extrusive and intrusive rocks with areal extents >0.1 Mkm^2 and volumes >0.25 Mkm^3 (Bryan, 2007; Bryan and Ernst, 2008; Bryan et al., 2002), are a recently recognized type of large igneous province (LIP) defined by Bryan et al. (2002). They have potentially important implications for geodynamic processes, economic resources (Bryan, 2007; Bryan and Ferrari, 2013; Pankhurst et al., 2011a), and the environment (Bryan, 2007).

During the last two decades, a significant number of SLIPs have been recognized including the Tertiary Sierra Madre Occidental of Mexico (Bryan et al., 2002), the Early Cretaceous Whitsunday igneous province (Bryan, 2007; Bryan et al., 1997, 2000), the Jurassic Chon Aike Province (Pankhurst et al., 1998, 2000), the Paleozoic Kennedy–Connors–Auburn province, northeast Australia (Bryan et al., 2003) and the Mesoproterozoic Gawler SLIP, southern Australia (Allen et al., 2008; Pankhurst et al., 2011b). These SLIPs are characterized by large volumes ($>10^5$ km^3), of predominantly rhyodacite–rhyolite compositions, long

periods of magmatic evolution (<40 myr) and were located along paleo- or active continental margins (Bryan, 2007; Bryan et al., 2002). Unlike the mafic LIPs commonly related to mantle plumes (e.g., Bryan and Ernst, 2008; Chung et al., 1998; Coffin and Eldholm, 1994; Ernst and Buchan, 2001, 2003), the mechanisms for the formation of the SLIPs are not as clear and the generation of SLIPs may be related to continental rifting, mantle plumes or back arc extension (Betts et al., 2009; Bryan, 2007; Bryan and Ferrari, 2013; Bryan et al., 2002; Pankhurst et al., 2000, 2011b).

Early Permian (ca. 280 Ma) igneous rocks with predominantly ultramafic–mafic rocks are widespread in the Tarim Craton and the Central Asian Orogenic Belt (CAOB) (e.g., Li et al., 2011; Wei et al., 2014; Xia et al., 2012; Xu et al., 2013; Yang et al., 2007, 2013; Zhang et al., 2010; Zhou et al., 2004, 2009), and correspond to the Tarim LIP (e.g., Qin et al., 2011; Su et al., 2011, 2012). Recent dating of rocks on the Alxa Block, adjacent to the Tarim Craton and the CAOB, reveals that a large area of Early Permian (ca. 280 Ma) granitoids occur in the Block (e.g., Geng and Zhou, 2012; Li, 2006; Shi et al., 2012). Thus, although they may represent a silicic igneous province, its area (0.05 Mkm^2) is smaller than a SLIP as defined by Bryan (2007) (>0.1 Mkm^2). However, the petrogenesis and the tectonic setting of these granitoids, and their relationship to the broadly contemporaneous Tarim LIP are unclear. In this contribution, we present in situ zircon U–Pb age and Hf–O isotope data and whole-rock element and Nd–Sr isotope data for two newly

identified rock associations from the Alxa Block: Early Permian I-type and A-type granites plus high Sr/Y granodiorites in the Bayannuoergong area, and gabbros, diorites and quartz diorites in Bijiertai Complex. Our work shows that a silicic igneous province corresponding to a ca. 280 Ma magmatic flare-up can be found in the Alxa Block, and suggest that the magmatic event was probably triggered by the contemporaneous Tarim mantle plume.
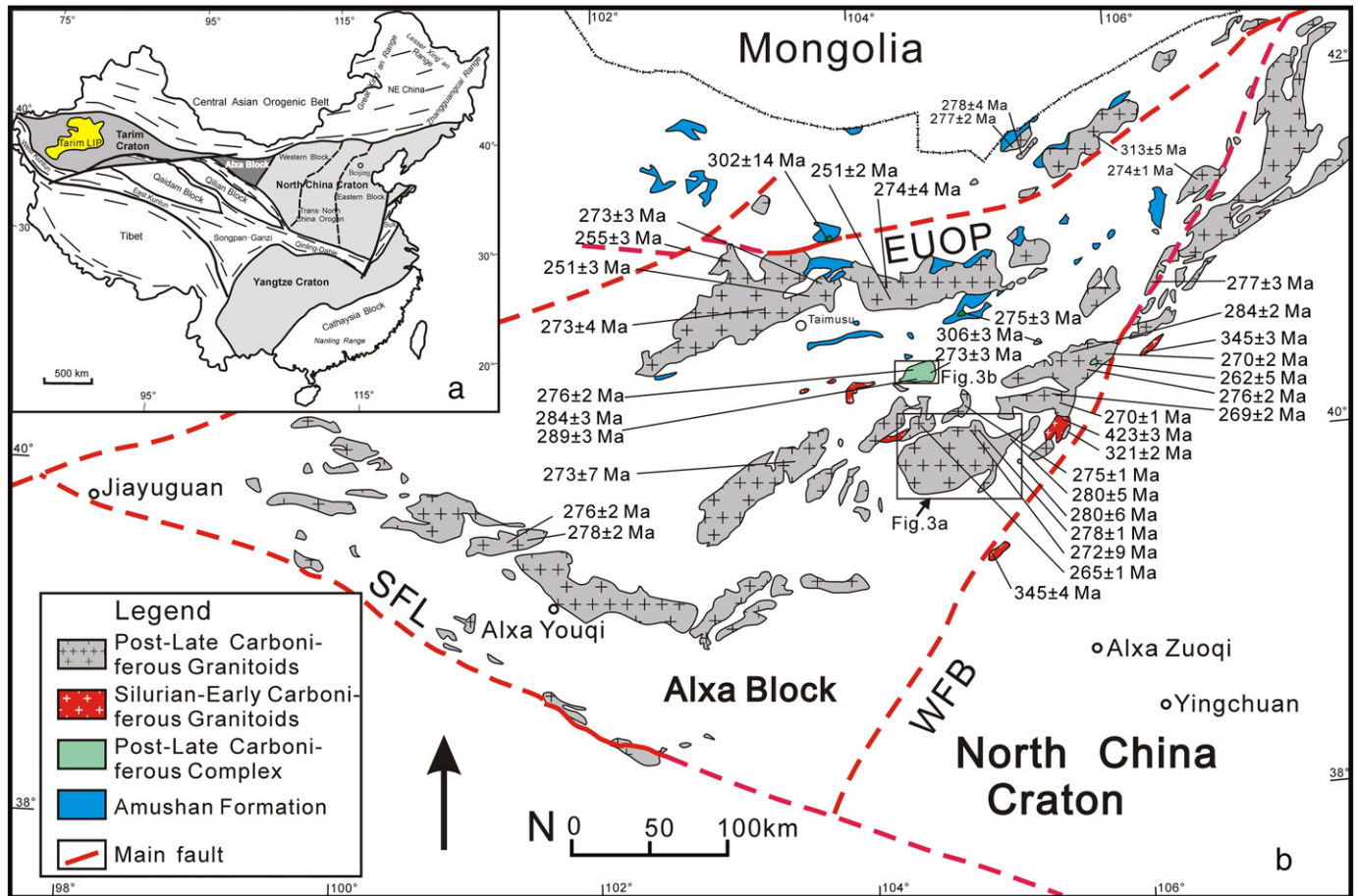
2. Geological setting

The Alxa Block, located in westernmost North China, connects the North China Craton, the Tarim Craton, the CAOB and the Qilian Block (Fig. 1a). It has recently been interpreted as an independent block by Dan et al. (2012, 2013, 2014), although it was previously thought to be a part of the North China Craton (NCC) (*e.g.*, NMBGMR (Nei Mongol Bureau of Geology and Mineral Resources), 1991; Zhao et al., 2005). The Alxa Block is bounded by the Late Paleozoic Enger Us Ophiolite Belt in the north, the western margin fault of Bayanwulashan in the east and the southern margin fault of Longshoushan in the south (Fig. 1b). It is largely covered by deserts, and outcrops of pre-Neoproterozoic crystalline basement rocks are only seen in the southwestern parts of the block. The oldest rocks are the newly discovered ~2.5 Ga tonalite–trondhjemite–granodiorite (TTG) exposed in the Beidashan Complex (Gong et al., 2012; Zhang et al., 2013a) and Paleoproterozoic rocks with ages of ~2.3–1.9 Ga exposed in the Longshoushan Complex that were metamorphosed at ~1.9 Ga and

~1.8 Ga (Gong et al., 2011; Tung et al., 2007). The Mesoproterozoic medium- to low-metamorphic grade Alxa Group (Geng et al., 2007) was unconformably covered by Neoproterozoic un-metamorphosed to very low-grade metamorphosed sedimentary sequences (NMBGMR (Nei Mongol Bureau of Geology and Mineral Resources), 1991; Chen et al., 2004). In the Neoproterozoic, a few S-type granites with ages of 930–910 Ma were intruded in the central Alxa Block (Dan et al., 2014; Geng et al., 2002).

A large volume of Phanerozoic granitoids are exposed in the Alxa Block (NMBGMR(Nei Mongol Bureau of Geology and Mineral Resources), 1991). Granitoids with ages >320 Ma are rare, however, and only a few are exposed near the eastern margin of the Alxa Block (Dan et al., 2013; Li, 2006). Recent studies suggest that they were mainly formed at 300–260 Ma (Fig. 1b) (Geng and Zhou, 2012; Lai et al., 2007; Li, 2006, 2012; Li et al., 2010a,2010b; Pi et al., 2010; Shi et al., 2012; Wu, 2011). However, the corresponding geochemical data are relatively scarce, and the petrogenesis and tectonic setting remain unclear.

Late Carboniferous–Early Permian volcanic rocks were discovered in the Upper Carboniferous–Lower Permian Amushan Formation. The formation is the oldest stratum in the Alxa Block and its age was established by LA–ICP-MS zircon dates of 320–302 Ma from the lower part of the formation (Lu et al., 2012). The lower and middle sections of the Amushan Formation consist of volcanic (mainly acid rocks and subordinate basic rocks), clastic, and carbonate rocks; the upper section is a molasse composed of silty shale, sandstone, gravel-bearing

Fig. 1. (a) Tectonic subdivision of China, (b) geological map showing the distribution of Phanerozoic granitoids and Amushan Formation in the Alxa Block and adjacent areas, Tarim LIP, Tarim large igneous province; SFL, southern margin fault of Longshoushan; WFB, western margin fault of Bayanwulashan; EUOB, Enger Us Ophiolite Belt.
Age sources in b: Li (2006); Lai et al. (2007); Li et al. (2010a, b); Wu (2011); Ran et al. (2012); Shi et al. (2012); Geng and Zhou (2012); Feng et al. (2013); Zhang et al. (2013b); Zheng et al. (2013).

sandstone and conglomerate (Lu et al., 2012). The basic rocks show affinities with intraplate magmatism, indicating that this formation was formed in a continental rifting setting (Dang et al., 2011; Jiang et al., 2011).

3. Regional geology

3.1. Bayannuoergong batholith

The Bayannuoergong batholith is one of the largest in the Alxa Block, and outcrops over 2000 km². It intruded into Precambrian strata and contains a few Precambrian xenoliths (Fig. 2a). The batholith consists mainly of coarse monzogranites and granodiorites, along with a few diorites and A-type granites (Fig. 2a), and some later felsic dykes (Fig. 2a). Mafic microgranular enclaves are commonly observed within the monzogranites, especially at pluton margins, and also occur within granodiorites. Recent LA–ICP-MS zircon U–Pb dating indicates that the emplacement ages of the monzogranites and granodiorites are 285–273 Ma (Li, 2012; Wu, 2011) and 265 Ma (Li, 2012), respectively.

The monzogranites and A-type granites consist of quartz (20–30 vol.%), alkali feldspar (20–30 vol.%), plagioclase (20–30 vol.%), biotite (0–10 vol.%), rare hornblende and accessory minerals (<1 vol.%), including zircon and apatite. The granodiorites consist of quartz (20–25 vol.%), alkali feldspar (10–20 vol.%), plagioclase (50–60 vol.%), biotite (5–15 vol.%), hornblende (3–5 vol.%) and accessory minerals, including zircon and apatite.

3.2. Bijiertai Complex

The Bijiertai Complex, about 35 km to the north of Bayannuoergong batholith, is composed mainly of Early Paleozoic gabbros, diorites, quartz diorites, granodiorites, granites and two mafic–ultramafic lenses within these rocks (Fig. 2b) (Feng et al., 2013; Geng and Zhou, 2012). Abundant gneissic sedimentary xenoliths with unknown-ages occur in the complex (Geng and Zhou, 2012). Recent LA–ICP-MS zircon U–Pb dating indicates that the diorites and granodiorites were formed at 288–276 Ma (Geng and Zhou, 2012), and the gabbro at 274 Ma (Feng et al., 2013).

The gabbros, diorites, and quartz diorites are studied in this paper. The gabbros are composed mainly of clinopyxene (60–65 vol.%), plagioclase (30–40 vol.%) and minor biotite (2 vol.%), the diorites consist mainly of hornblende (30–40 vol.%), plagioclase (45–55 vol.%) and quartz (<5 vol.%), and the quartz diorites consist of hornblende (10–20 vol.%), plagioclase (60–75 vol.%) and quartz (5–10 vol.%). In contrast to the medium-grained gabbros and diorites, the quartz diorites are coarse-grained, and the plagioclases show cumulative texture.

4. Analytical procedures

4.1. Zircon U–Pb dating

Measurements of U, Th and Pb for samples 09AL22-1, 09AL27, 09AL33 and 09AL70 were conducted using the Cameca IMS-1280 SIMS at the Institute of Geology and Geophysics, Chinese Academy of Sciences (IGG-CAS), Beijing. U–Th–Pb ratios and their absolute abundances were determined relative to the standard zircon Plešovice (Sláma et al., 2008) and 91500 (Wiedenbeck et al., 1995), respectively, using operating and data processing procedures similar to those described by Li et al. (2009, 2010c). Uncertainties on individual analyses in the data tables are reported at a 1σ level. Mean ages for pooled U/Pb and Pb/Pb analyses are quoted with 2σ and/or 95% confidence intervals. The weighted mean U–Pb ages and Concordia plots were processed using an Isoplot/Ex v.3.0 program (Ludwig, 2003). SIMS zircon U–Pb isotopic data are presented in Supplementary Table A.1.

The LA–ICP-MS U–Pb dating for samples 09AL12-3, 09AL37 and 09AL73 was conducted using an Agilent 7500a ICP-MS with an attached 193 nm excimer ArF laser-ablation system (GeoLas Plus) at IGG-CAS. The analytical procedures are similar to those described by Xie et al. (2008). $^{207}Pb/^{206}Pb$ and $^{206}Pb/^{238}U$ ratios were calculated using the ICPMSDataCal software (Liu et al., 2010a, 2010b), using the zircon standard 91500 as an external standard. Common Pb was corrected according to the method proposed by Andersen (2002). The weighted mean U–Pb ages and Concordia plots were processed using the Isoplot/Ex v.3.0 program (Ludwig, 2003). Analyses of the zircon standard GJ-1 as an unknown yielded a weighted mean $^{206}Pb/^{238}U$ age of 606 ± 4 Ma (2σ, n = 25), which is in good agreement with the recommended value (Jackson et al., 2004). LA–ICP-MS zircon U–Pb isotopic data are presented in Supplementary Table A.1.

4.2. Zircon oxygen isotopes

Zircon oxygen isotopes were measured using the same Cameca IMS-1280 SIMS at IGG-CAS. The detailed analytical procedures were similar to those described by Li et al. (2010d). The measured oxygen isotopic data were corrected for instrumental mass fractionation (IMF) using the Penglai zircon standard ($\delta^{18}O_{VSMOW}$ = 5.3‰) (Li et al., 2010e).
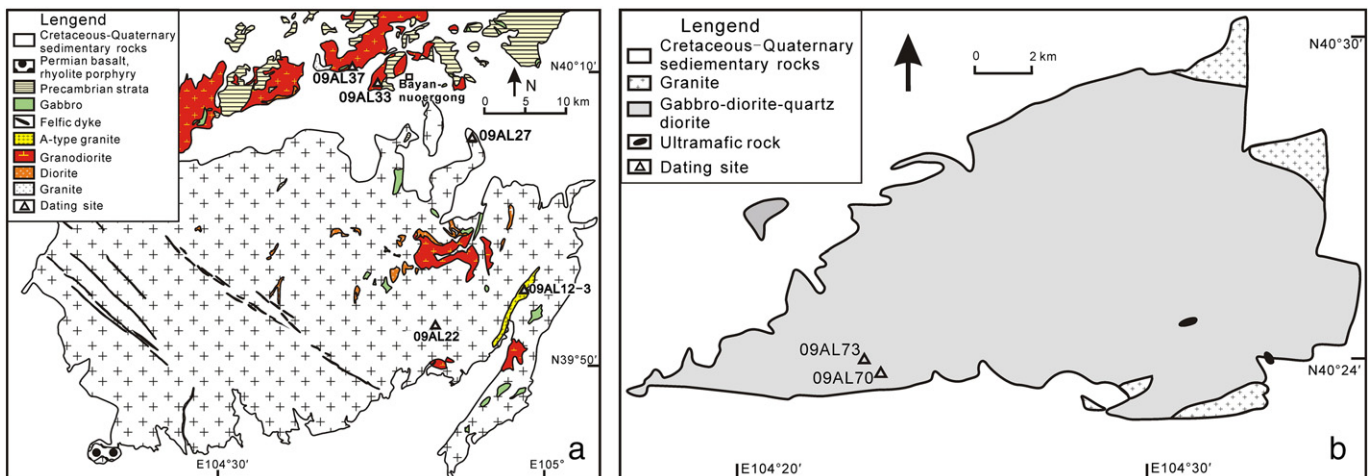

Fig. 2. (a) Geological sketch-map of the Bayannuoergong batholith (NMBGMR(Nei Mongol Bureau of Geology and Mineral Resources), 1991) and (b) Bijiertai Complex, with locations of dating samples.

The internal precision of a single analysis generally was better than 0.2‰ (1σ standard error) for the $^{18}O/^{16}O$ ratio. The external precision, measured by the reproducibility of repeated analyses of the Penglai standard, is 0.41‰ (2SD, n = 120). Ten measurements of the 91500 zircon standard during the course of this study yielded a weighted mean of $\delta^{18}O = 10.2 \pm 0.5$‰ (2SD), which is consistent within errors with the reported value of 9.9 ± 0.3‰ (Wiedenbeck et al., 2004). Zircon oxygen isotopic data are listed in Supplementary Table A.2.

4.3. Zircon Lu–Hf isotopes

In situ zircon Lu–Hf isotopic analyses were carried out on a Neptune multi-collector ICP-MS equipped with a Geolas-193 Geolas 2005 excimer ArF laser ablation system at the State Key Laboratory of Geological Processes and Mineral Resources, China University of Geosciences in Wuhan. Lu–Hf isotopic analyses were conducted on the same zircon grains that were previously analyzed for U–Pb and O isotopes. Detailed analytical procedures were similar to those described by Hu et al. (2012). Measured $^{176}Hf/^{177}Hf$ ratios were normalized to $^{179}Hf/^{177}Hf = 0.7325$. Further external adjustment was not applied for the unknowns because our determined $^{176}Hf/^{177}Hf$ ratios for zircon standards 91500 (0.282308 ± 0.000004) and GJ-1 (0.282021 ± 0.000011) were in good agreement within errors with the reported values (Griffin et al., 2006; Wu et al., 2006; Zeh et al., 2007). Zircon Hf isotopic data are listed in Supplementary Table A.2.

4.4. Major and trace elements

Sixteen powdered rock samples of ~200-mesh size were used for geochemical analyses. Major element oxides were analyzed on fused glass beads using a Rigaku RIX 2000 X-ray fluorescence spectrometer at the State Key Laboratory of Isotope Geochemistry, the Guangzhou Institute of Geochemistry, Chinese Academy of Sciences (SKLaBIG GIG CAS). Calibration lines used in quantification were produced by bivariate regression of data from 36 reference materials encompassing a wide range of silicate compositions (Li et al., 2005). Analytical uncertainties are between 1% and 5%. Trace elements were analyzed using an Agilent 7500a ICP-MS at GIG CAS. Analytical procedures were similar to those described by Li et al. (2000). A set of USGS and Chinese national rock standards, including BHVO-2, GSR-1, GSR-2, GSR-3, AGV-2, W-2 and SARM-4 were chosen for calibration. Analytical precision typically is better than 5%. Geochemical results are listed in Supplementary Table A.3.

4.5. Sr and Nd isotopic compositions

Sixteen samples were selected for whole rock Rb–Sr and Sm–Nd isotopic analyses (Supplementary Table A.4). Sr–Nd isotopic compositions were determined using a Micromass Isoprobe multi-collector ICP-MS at SKLIG GIG CAS, and analytical procedures described by Li et al. (2004). Sr and Nd were separated using cation columns, and Nd fractions were further separated by HDEHP-coated Kef columns. The measured $^{87}Sr/^{86}Sr$ ratio of the NBS 987 standard and $^{143}Nd/^{144}Nd$ ratio of the JNdi-1 standard were 0.710274 ± 18 (n = 11, 2σ) and 0.512093 ± 11 (n = 11, 2σ), respectively. All measured Nd and Sr isotope ratios were normalized to $^{146}Nd/^{144}Nd = 0.7219$ and $^{86}Sr/^{88}Sr = 0.1194$, respectively. The Sr–Nd isotope results are listed in Supplementary Table A.4.

5. Results

5.1. Zircon U–Pb dating results

Zircon grains separated for dating are mostly euhedral to subhedral, with lengths of ~100–250 μm, and length to width ratios of 2:1 to 4:1. The oscillatory zoning cathodoluminescence images in most grains

and high Th/U ratios (0.12–1.04) (Supplementary Table A.1), suggest magmatic origins (Belousova et al., 2002). SIMS was used to date all samples except for samples 09AL12-3, 09AL37 and 09AL73, which were dated by LA–ICP-MS. U–Pb concordia diagrams of analyzed zircons are shown in Fig. 3, and the U–Pb age data are given in Supplementary Table A.1.

Seven samples were selected for dating. Samples 09AL22-1 and 09AL27 are monzogranites and give weighted mean $^{206}Pb/^{238}U$ ages of 278 ± 2 and 284 ± 3 Ma, respectively (Fig. 3a, b). Sample 09AL12-3 is an A-type granite and produces a weighted mean $^{206}Pb/^{238}U$ age of 279 ± 2 (Fig. 3c). Samples 09AL33 and 09AL37 are granodiorites and have weighted mean $^{206}Pb/^{238}U$ ages of 281 ± 2 Ma and 283 ± 2 Ma, respectively (Fig. 3d, e). Samples 09AL70 and 09AL73 are diorites and quartz diorites, respectively. They give weighted mean $^{206}Pb/^{238}U$ ages of 280 ± 2 (Fig. 3f) and 282 ± 2 (Fig. 3 g), respectively.

In summary, the zircon U–Pb age data indicate that the granitoids in the Bayannuoergong batholith and the diorites and quartz diorites in the Bijiertai Complex were all formed at ca. 280 Ma (284–278 Ma).

5.2. Whole-rock major and trace element compositions

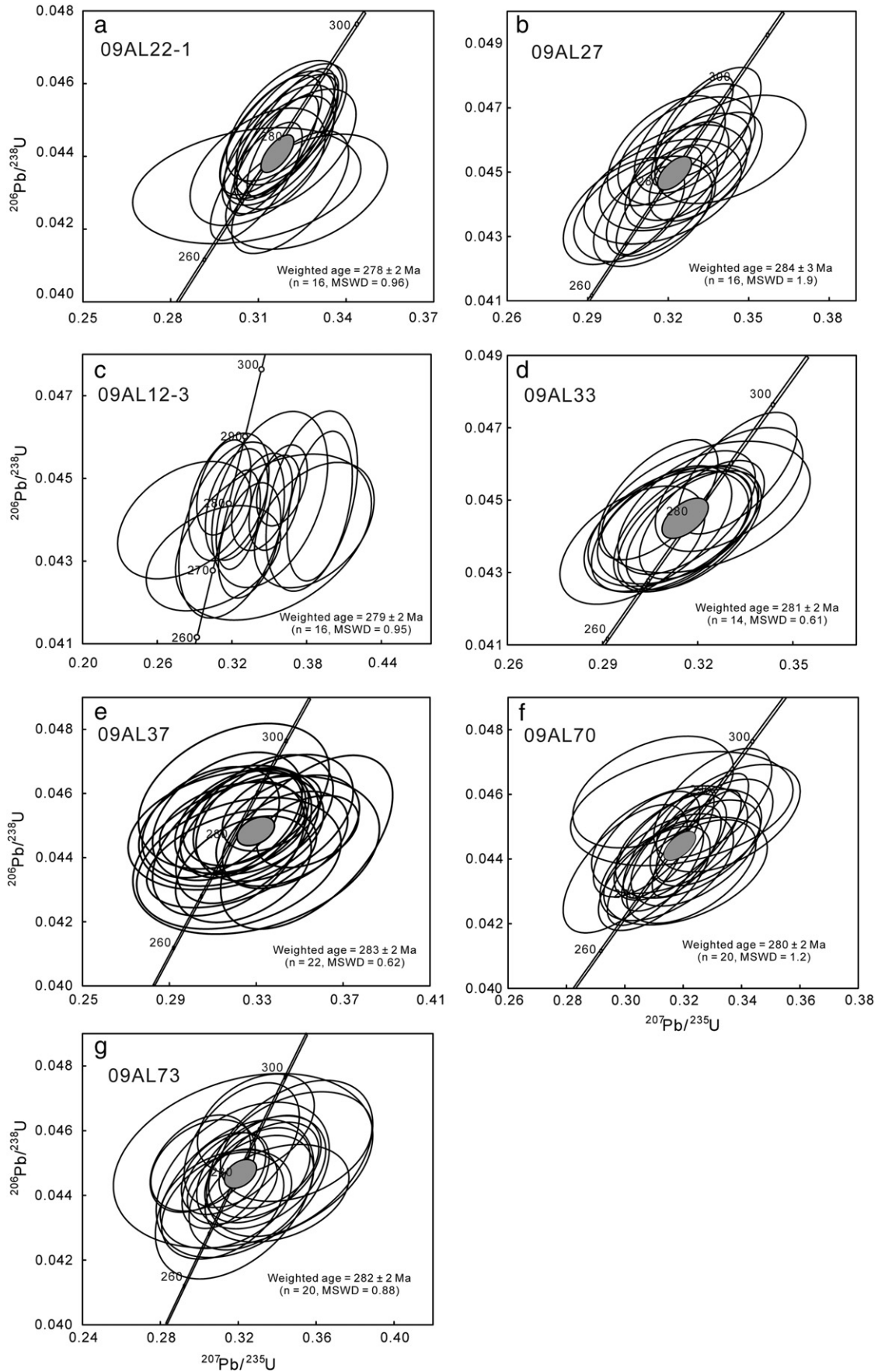#### 5.2.1. The granitoids from Bayannuoergong batholith

The monzogranites from Bayannuoergong batholith are high in silica and alkalis, with SiO_2 ranging from 69.5 to 78.6 wt.% (volatile-free) and total $K_2O + Na_2O$ contents varying from 7.0 to 8.7 wt.% (Supplementary Table A.3). The granodiorites have slightly lower silica and alkali contents with SiO_2 ranging from 63.6 to 66.6 wt.% and total $K_2O + Na_2O$ varying from 5.3 to 6.0 wt.% (Supplementary Table A.3). The monzogranites and granodiorites are subalkaline on the alkali *versus* silica diagram (Fig. 4a). They have lower TiO_2, $Fe_2O_3^T$, MnO, MgO, CaO, and P_2O_5 contents (Supplementary Table A.3), but higher Th and $(Na_2O + K_2O)/CaO$ than the gabbro, diorite and quartz diorite from the Bijiertai Complex (Fig. 5). The A-type granites (09AL12-1, 09AL12-2 and 09AL12-3) have high SiO_2 (78.5–78.6 wt.%), alkalis ($Na_2O + K_2O = 8.2–8.5$ wt.%) and FeO^T/MgO ratios, and low CaO, MgO contents (Fig. 5; Supplementary Table A.3).

Chondrite-normalized REE patterns of the monzogranites and granodiorites (Fig. 4b) show relative enrichment of light rare earth elements (LREEs), with variable $(La/Yb)_N$ ratios (3–58). The monzogranites are characterized by significant negative Eu anomalies, whereas the granodiorites display negligible Eu anomalies. Five monzogranites (09AL18-1, 09AL18-2, 09AL19-1, 09AL19-2, 09AL21) show heavy rare earth element (HREE) depletion, with high $(La/Yb)_N$ ratios (16–58). Three samples (09AL12-1, 09AL12-2, 09AL12-3) show negative anomalies in Ba, Nb, Ta, Sr, P, Eu and Ti (Fig. 4c), characteristics of A-type granites (*e.g.*, Eby, 1990, 1992; Yang et al., 2006). The HREE abundances of the granodiorites are lower than those of the monzogranites. Furthermore, the granodiorites are characterized by relatively high Sr but low Yb and Y contents with high Sr/Y ratios of 22–71, similar to those of modern adakites and Archean TTG suites (Fig. 4d) (*e.g.*, Defant and Drummond, 1990; Martin et al., 2005).
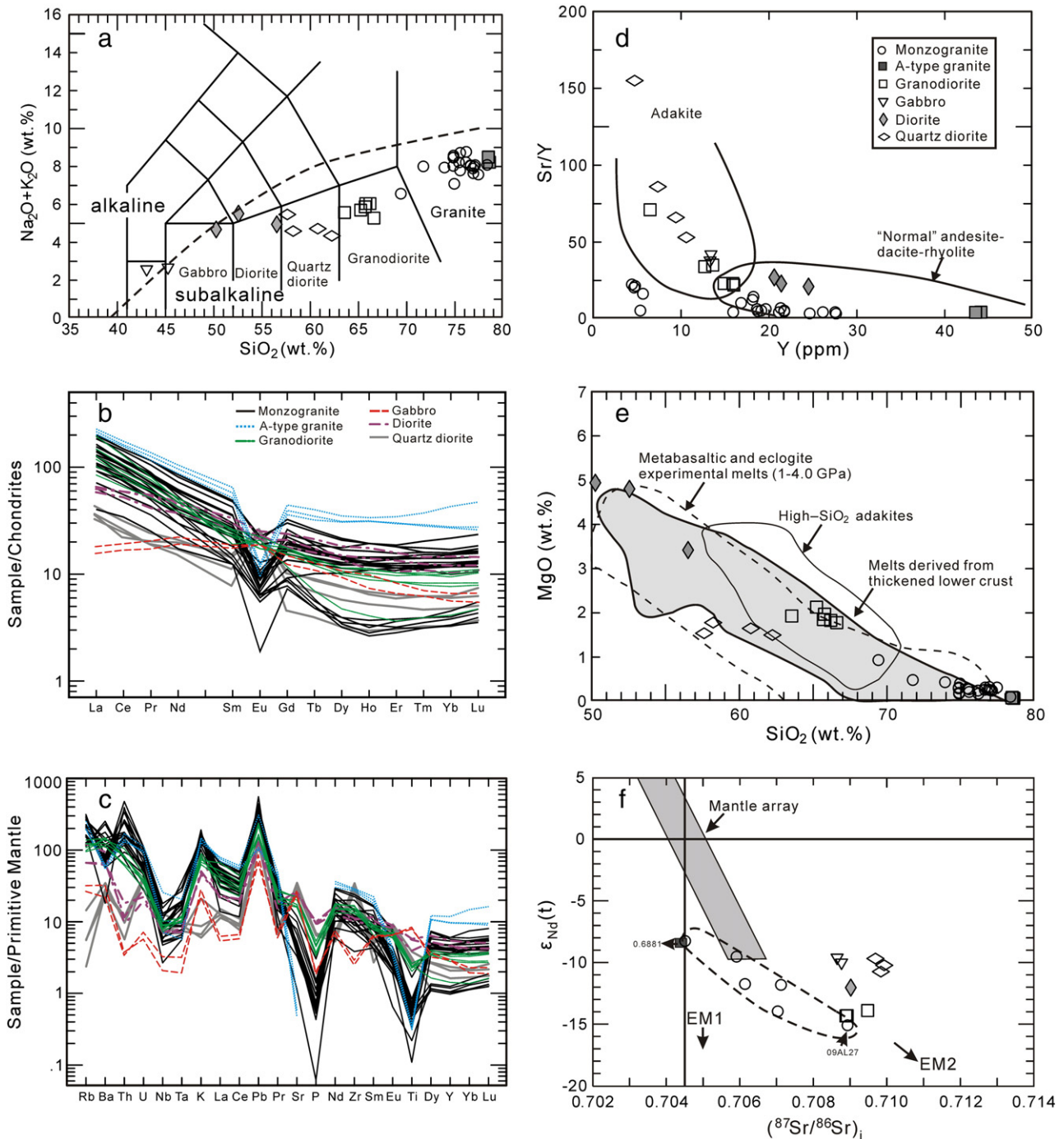
5.2.2. Bijiertai Complex: gabbro, diorite and quartz diorite

The gabbros, diorites and quartz diorites have SiO_2 contents of 43.0–45.3 wt.%, 50.3–56.5 wt.% and 57.6–62.2 wt.%, respectively. The gabbros have high $Mg^{\#}$ values of 64.5–66.4, but the diorites and quartz diorites have lower $Mg^{\#}$ values of 47.1–52.1 and 38.1–40.1, respectively. All three rock types plot in the subalkaline field on the alkali *versus* silica diagram (Fig. 4a).

All of these rocks are enriched in LREE. The gabbros and diorites have negligible Eu anomalies, whereas quartz diorites have significant positive Eu anomalies. Gabbros show nearly flat LREE and fractionated HREE patterns with significant negative Ta and Nb anomalies. The quartz diorites are characterized by high Sr but low Yb and Y contents with high Sr/Y ratios of 53–155 (Supplementary Table A. 3).

Fig. 3. *In situ* U–Pb dating results for the Early Permian rocks in Alxa Block. (a, b) Monzogranites (09AL22-1 and 09AL27), (c) A-type granite (09AL12-3), (d, e) granodiorites (09AL33 and 09AL37), (f) diorite (09AL70) and (g) quartz diorite (09AL73). Data-point error ellipses are 2σ.

Fig. 4. (a) SiO_2 *vs.* $K_2O + Na_2O$ diagram for intrusive rocks (Middlemost, 1994); (b) chondrite-normalized REE diagrams and (c) primitive mantle- normalized incompatible trace element diagrams for the Early Permian rocks, and the normalization values are from Sun and McDonough (1989); (d) Sr/Y *vs.* Y diagram (after Defant et al., 2002); (e) SiO_2 *vs.* MgO diagram. The field of metabasaltic and eclogite experimental melts (1–4.0 GPa) is from the following references: Sen and Dunn (1994); Rapp and Watson (1995); Springer and Seck (1997); Rapp et al. (1999); Skjerlie and Patiño Douce (2002), and references therein. Fields of adakites inferred to be derived from subducting oceanic crust is after Wang et al. (2006). Melts formed by partial melting of the lower mafic crust are from the following references: Atherton and Petford (1993); Chung et al. (2003); Johnson et al. (1997); Muir et al. (1995); Petford and Atherton (1996); Wang et al. (2005). (f) Nd–Sr isotope composition for the Early Permian igneous rocks. EMI, I-type enriched mantle, EMII, II-type enriched mantle (Zindler and Hart, 1986).

5.3. Whole rock Sr–Nd isotopic compositions

The monzogranites exhibit the lowest and most variable initial $^{87}Sr/^{86}Sr$ isotopic ratios and highly variable $\varepsilon_{Nd}(t)$ values (Fig. 4f), corresponding to two-stage Nd model ages (T_{2DM}) of 2.27–1.72 Ga. The granodiorites have higher initial $^{87}Sr/^{86}Sr$ isotopic ratios (0.70889–0.70948) and $\varepsilon_{Nd}(t)$ values of −14.3 to −13.8,

corresponding to a T_{2DM} of 2.21–2.17 Ga. The A-type granite has the highest $\varepsilon_{Nd}(t)$ value of −8.4, corresponding to a T_{2DM} of 1.74 Ga. The gabbros, diorites and quartz diorites from the Bijiertai Complex have initial $^{87}Sr/^{86}Sr$ isotopic ratios ranging from 0.7086 to 0.7098, and $\varepsilon_{Nd}(t)$ values ranging from −12.0 to −9.5. The monzogranites exhibit a significant negative correlation between $\varepsilon_{Nd}(t)$ values and $(^{87}Sr/^{86}Sr)_i$ ratios (Fig. 4f).
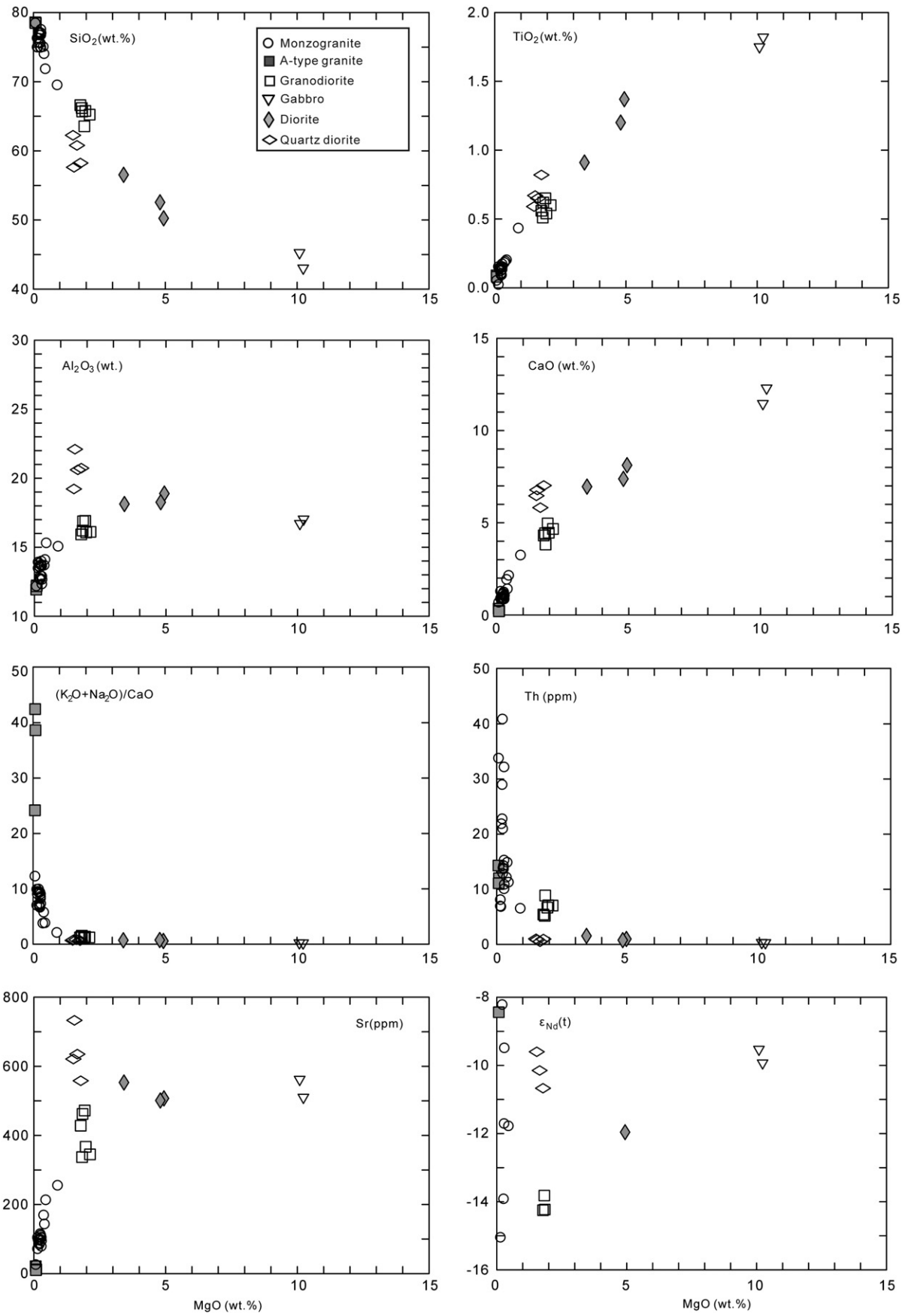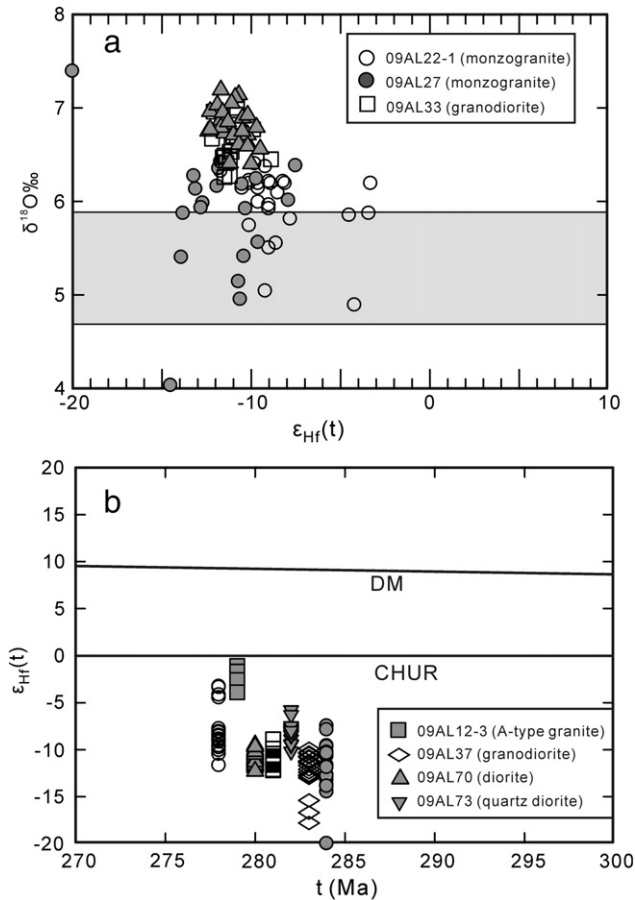
Fig. 5. Selected major oxide (wt.%) and trace elements (ppm) *vs.* SiO$_2$ (wt.%) for the Early Permian rocks.

Fig. 6. Plots of (a) $\varepsilon_{Hf}(t)$ values vs. $\delta^{18}O$ values and (b) $\varepsilon_{Hf}(t)$ values vs. crystallization ages for the magmatic zircons from the Early Permian igneous rocks. The shaded field depicts the $\delta^{18}O$ value (5.3 ± 0.6‰, 2SD) of the mantle-derived zircons.

5.4. Zircon Hf–O isotopic compositions

In situ LA–MC–ICP-MS Lu–Hf isotopic analyses were conducted on the zircon grains that were previously analyzed for U–Pb and/or O isotopes. Their results are presented in Supplementary Table A.2 and Fig. 6. The monzogranites (samples 09AL22-1 and 09AL27) and granodiorites (09AL33 and 09AL37) have a large range of $\varepsilon_{Hf}(t)$ values of −17.8 to −3.3 (one point is −20.0), corresponding to two-stage zircon Hf model ages (T_{DM}^C) of 2.43–1.51 Ga (one point is 2.56 Ga). The diorite (09AL70), quartz diorite (09AL73) and A-type granite (09AL12-3) have a smaller range of age-corrected $\varepsilon_{Hf}(t)$ values (Fig. 6b, Supplementary Table A.2), corresponding to T_{DM}^C of 2.08–1.90 Ga, 1.95–1.67 Ga and 1.55–1.37 Ga, respectively. Most of the two-stage zircon Hf model ages are 2.2–1.8 Ga, but samples 09AL12-3 (A-type granite) and 09AL22-1 (monzogranite) give ages between 1.6 and 1.4 Ga. It is noted that the A-type granites have the highest $\varepsilon_{Hf}(t)$ values among these rocks.

Zircon O isotopes were analyzed on the diorite, granodiorite and monzogranite. The measured $\delta^{18}O$ values for zircons from the diorite (09AL70) and granodiorite (09AL33) show similar and limited ranges forming normal Gaussian distributions, with averaged values of 6.80 ± 0.21‰ (1SD) and 6.61 ± 0.21‰ (1SD), respectively (Fig. 7). Measured zircon $\delta^{18}O$ values for the monzogranites show a few anomalous spots. For sample 09AL22-1, spots show a limited range of 5.5–6.4‰, with a peak of 6.2‰, except for two anomalous spots at 4.9 and 5.0‰ (Fig. 7). For sample 09AL27, most spots show a slightly large range of 5.0–6.4‰, with a peak of 6.2‰, apart from two spots with anomalous values of 4.0‰ and 7.4‰ (Fig. 7).

6. Discussion

6.1. Ca. 280 Ma magmatic flare-up in the Alxa Block

To better understand the petrogenesis and tectonic significance of the Permian magmatic rocks in the Alxa Block, we carried out a regional data compilation (Supplementary Table A.5). Fig. 1b shows the representative Permian igneous rocks in the Alxa Block, marked with representative ages. Fig. 8 shows the frequency distribution of the known Paleozoic igneous ages from the Alxa Block and adjacent areas using Isoplot (Ludwig, 2003), highlighting peak activities at ~278 Ma. The Paleozoic magmatism can be broadly divided into three main episodes encompassing the Silurian to Early Carboniferous (424–337 Ma), the Late Carboniferous (320–300 Ma) and the Permian (290–250 Ma). The Silurian to Early Carboniferous igneous rocks are distributed in the eastern margin of the Alxa Block and adjacent areas (Fig. 1b) and are probably caused by Paleozoic orogenesis in the eastern Alxa Block (Dan et al., 2013). The Late Carboniferous magmatic rocks consist mainly of volcanic rocks and are distributed in the northern Alxa Block and adjacent areas (Fig. 1b) and were possibly generated in an intraplate setting (Dang et al., 2011; Jiang et al., 2011).

The Permian igneous rocks are largely distributed in the Alxa Block and adjacent areas. Most of them were formed at ca. 290–270 Ma, with a peak age of ~278 Ma (Fig. 8). This period of igneous activity is characterized by voluminous granites rather than mafic rocks (Supplementary Table A.5). Although the rocks are distributed over an area of 0.15 Mkm², the total area of outcrop (0.05 Mkm²) does not meet the 0.10 Mkm² threshold required for classification as a SLIP (Bryan, 2007; Bryan et al., 2002). Therefore, they cannot be classified as a SLIP at present. However, it is significant that the adjacent and areally extensive Upper Carboniferous–Lower Permian Amushan Formation in the northern Alxa Block contains large exposures of andesitic to rhyolitic volcanic rocks (Dang et al., 2011). Establishing whether or not they are a part of the Alxa silicic igneous province requires more high-precision geochronological data.

6.2. Petrogenesis of the ca. 280 Ma magmatic rocks

6.2.1. Bayannuoergong batholith

6.2.1.1. The monzogranites. Two end-member mixing may have played an important role in the generation of the monzogranites, based on the following lines of evidence. Their Nd isotopes negatively correlate with ($^{87}Sr/^{86}Sr)_i$ (Fig. 4f), and there is a negative correlation between Ba/La and $\varepsilon_{Nd}(t)$ (Fig. 9a). Sample 09AL27 has the most enriched isotopic compositions ($\varepsilon_{Nd}(t) = −15.1$ and ($^{87}Sr/^{86}Sr)_i = 0.7090$) and the highest Ba/La value (41.8), which is likely to be most representative of a lower crustal end-member component. The sample 09AL10-1 has the most depleted isotopic compositions ($\varepsilon_{Nd}(t) = −8.2$ and ($^{87}Sr/^{86}Sr)_i = 0.7045$) and the lowest Ba/La value (16.2), indicating that it likely corresponds closely to the other end-member component. Considering the relatively high Nd and low Sr isotopic values, this end-member component is proposed to be the lithospheric mantle. The fact that many zircons have mantle-like oxygen values is consistent with this suggestion (Fig. 6a). However, no coeval basaltic rocks were reported in the Bayannuoergong batholith, and therefore more data is required in order to constrain the proportion of the mantle component in the Bayannuoergong monzogranites.

A few anomalous values of zircon oxygen isotopes obtained from samples 09AL22-1 and 09AL27 suggest that some other materials were added to their sources or that their magmas underwent contamination. The low zircon oxygen isotopic value (4.0‰) (Fig. 7a), confirmed by duplicate analyses, is obviously lower than mantle zircon O values (5.3 ± 0.6‰) (Valley, 2003). Thus, one or more components that have undergone high-temperate water–rock interaction were added to the source of the monzogranites or contaminated their magmas. This
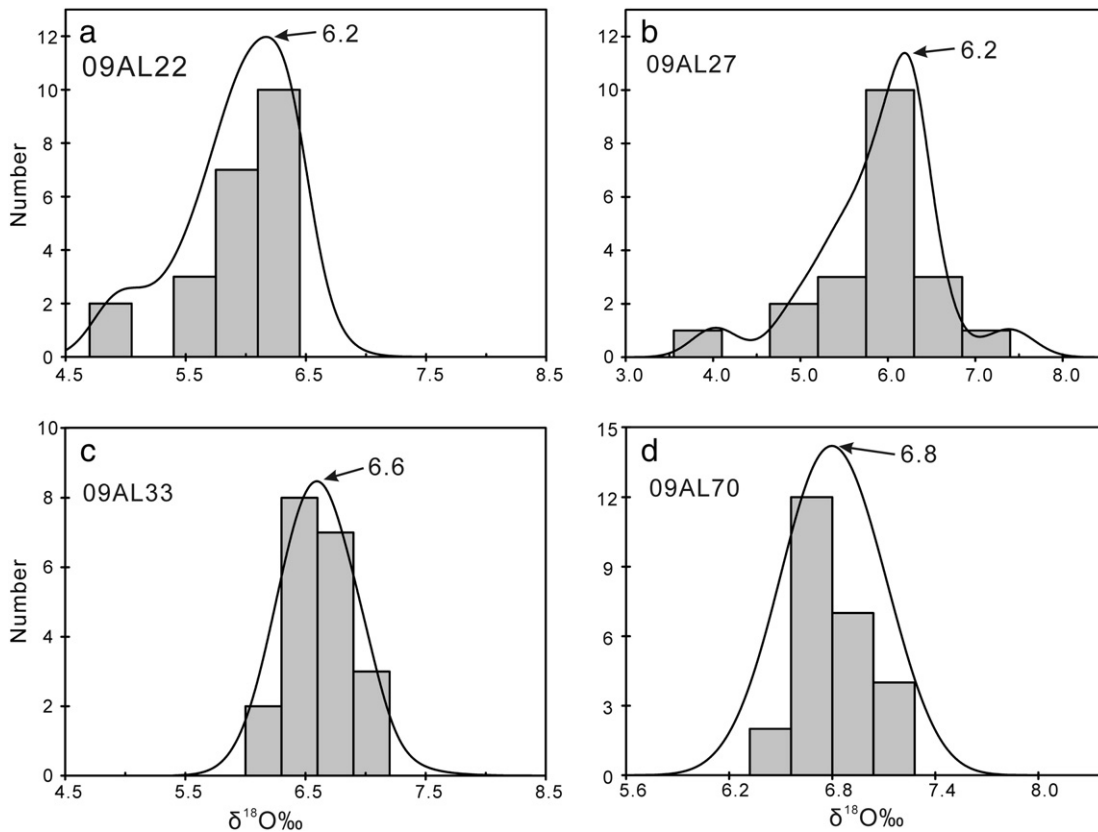
Fig. 7. Probability plots of zircon $\delta^{18}O$ values for the Early Permian igneous rocks.

material is the most plausibly basalt that had undergone high-temperature alteration in an oceanic setting. A high zircon O value (7.4‰) indicates that some other material was also added to the I-type monzogranite. These materials were probably Precambrian sedimentary rocks, as these are found as xenoliths in the monzogranites. This suggestion is consistent with the high Hf mantle model age (2.56 Ga) of this zircon grain (Supplementary Table A.2).

A few monzogranite samples display middle REE depletion (Fig. 4b). The concave REE patterns indicate that amphibolites may have been retained in their sources or were removed by crystal fractionation during magma evolution. These monzogranites have Sr–Nd isotopic compositions similar to the other monzogranites (Fig. 4f), suggesting that they have similar sources.

Fig. 8. Cumulative age spectra of the Paleozoic igneous rocks in Alxa Block. Data sources are in Supplementary Table A.5.

6.2.1.2. Occurrence of A-type granite in the Bayannuoergong batholith. Although many ~280 Ma granitoids have been reported in the Alxa Block, no A-type granitoids have been identified in previous studies. In general, A-type granites are comparatively enriched in high field strength elements (HFSEs), such as Zr, Nb, Y, REE and Ga (*e.g.*, Collins et al., 1982; Eby, 1992; King et al., 1997, 2001; Sylvester, 1989; Whalen et al., 1987; Yang et al., 2006). In this study, a few granites in the Bayannuoergong batholith have the characteristics of A-type gran-ites. Samples 09AL12-1, 09AL12-2 and 09AL12-3 have high $K_2O +$ Na_2O, Zr, FeO^T/MgO and Ga/Al ratios. On discrimination diagrams (Fig. 10a, b), they plot in the A-type granite field. Moreover, they show zircon saturation temperatures (849–854 °C) higher than those (683–833 °C) of other monzogranites (Fig. 10c). We therefore conclude that the three samples described in this study are A-type granites.

The origins of A-type granites have been attributed to: (1) direct frac-tionation of mantle-derived alkaline basalts (*e.g.*, Mushkin et al., 2003; Turner and Rushmer, 2009; Turner et al., 1992); (2) partial melting of crustal materials at high temperature (*e.g.*, Collins et al., 1982; King et al., 1997; Wang et al., 2010a) and (3) hybridization between anatectic crust-derived felsic and mantle-derived mafic magmas (*e.g.*, Kerr and Fryer, 1993; Mingram et al., 2000; Yang et al., 2006). The absence of any mafic microgranular enclaves in the A-type pluton does not support the generation of these A-type granites by mixing of mantle-derived mafic magma and crustal-derived silicic melts. The A-type granite has a high $\varepsilon_{Nd}(t)$ value, similar to the end-member component of the monzogranites with the highest $\varepsilon_{Nd}(t)$ values (Fig. 4f). Thus, it is difficult to distinguish a potential mantle-derived origin from the alternative origin *via* partial melting of crustal materials. The lack of coeval, proximal mafic rocks or rocks with intermediate compositions, their high SiO_2 contents relative to other ~280 Ma magmatic rocks, and their relatively low zircon saturation temperatures (~850 °C) compared to the 900–1100 °C temperatures calculated for mantle-derived A-type granites (*e.g.*, Pankhurst et al., 2011a; Turner and Rushmer, 2009; Turner et al.,
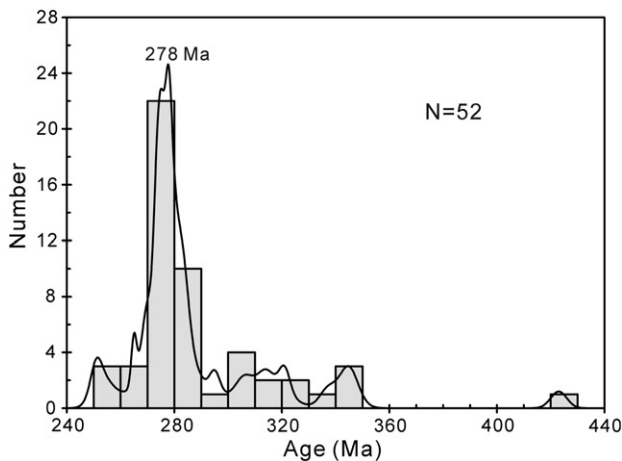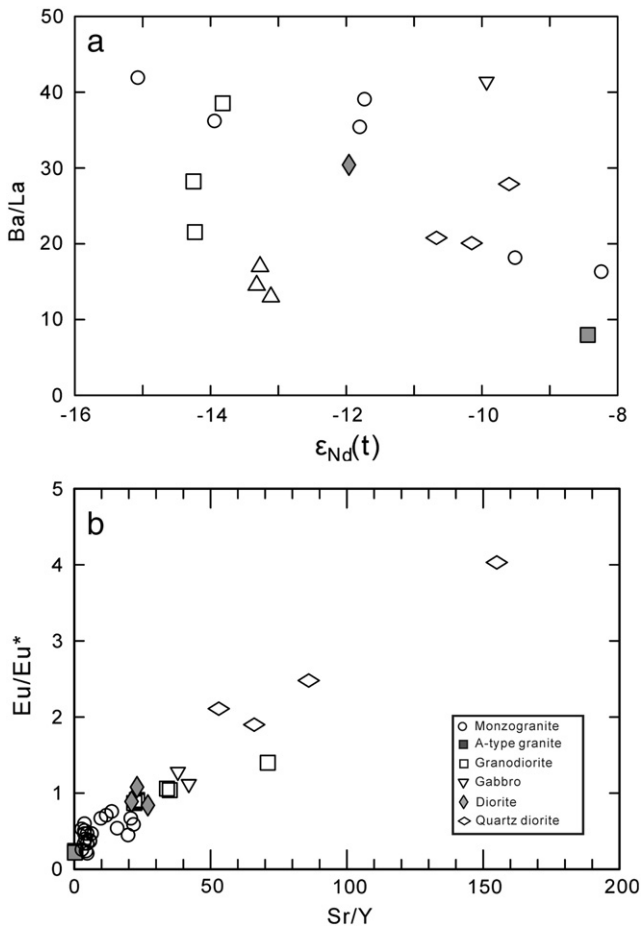
Fig. 9. Plots of (a) Ba/La vs. $\varepsilon_{Nd}(t)$ values, (b) Eu/Eu* vs. Sr/Y from the Early Permian igneous rocks.

1992) do not support a mantle-derived origin for the A-type granites. Therefore, their A_2 group affinities (Fig. 10d) imply that the magmas were derived from continental crust or underplated basaltic protoliths (Eby, 1992). The fact that the A-type granites have high zircon $\varepsilon_{Hf}(t)$ and whole rock $\varepsilon_{Nd}(t)$ values, similar to the high $\varepsilon_{Hf}(t)$ of I-type monzogranite end-member (Fig. 4f), indicates that the A-type granites were most plausibly generated by partial melting of the underplated mafic rocks.

6.2.1.3. High Sr/Y granodiorites. Although the granodiorites show some geochemical affinities with the "classical" adakites defined by Defant and Drummond (1990) (Fig. 4d), their K_2O/Na_2O ratios (0.58-0.80) are higher than those of typical adakites (K_2O/Na_2O ratios = 0.42) (Richards and Kerrich, 2007). Thus, they should be classed as high Sr/Y granites (Moyen, 2009). Several models have been proposed for the generation of high Sr/Y granitoids, including (a) melting of subducted young and hot oceanic crust (Defant and Drummond, 1990; Kay et al., 1993; Martin et al., 2005; Stern and Kilian, 1996; Tang et al., 2010a; Wang et al., 2007a, 2008); (b) assimilation and fractional crystallization (AFC) or fractional crystallization (FC) from parental basaltic magmas (Castillo et al., 1999; Macpherson et al., 2006; Richards and Kerrich, 2007; Rooney et al., 2011); (c) magma mixing between felsic and basaltic magmas (Guo et al., 2007; Streck et al., 2007); and (d) partial melting of thickened lower crust (Atherton and Petford, 1993; Chung et al., 2003; Petford and Atherton, 1996; Wang et al., 2005, 2007b).

In the case of the Alxa Block, the first three models cannot account for the petrogenesis of the granodiorites. Oceanic slab melting is

unlikely to have generated these high Sr/Y granitoids because of the apparent lack of contemporaneous subduction in the eastern Alxa Block and a slab source is inconsistent with their evolved Sr–Nd–Hf isotopic compositions (Figs. 3f and 5b). In addition, they have lower $Mg^{\#}$ (42–47) values than those (47–56) of metabasaltic rock-derived experimental melts contaminated by mantle peridotites (e.g., Rapp et al., 1999), indicating that the interaction between felsic magmas and mantle peridotites was unlikely. Additionally, their high $\delta^{18}O$ values of zircon (6.61 ± 0.21‰ (1SD)) (corresponding to a calculated whole-rock magmatic $\delta^{18}O$ value of 8.2‰) are not consistent with the mantle-like $\delta^{18}O$ values of the best global examples of slab-derived adakites (Bindeman et al., 2005). Mantle-derived magmatic suites generated by FC processes generally exhibit a continuous compositional trend from basaltic rocks to felsic rocks derived from residual magmas (e.g., Castillo et al., 1999; Macpherson et al., 2006; Richards and Kerrich, 2007). The absence of contemporaneous basaltic rocks associated with these granitoids rules out this mechanism. Rocks formed by magma mixing are usually intermediate in composition and have high Mg (e.g., adakitic high-Mg andesites) (Guo et al., 2007; Streck et al., 2007) rather than acidic adakitic compositions in this study. Additionally, the homogenous O and Hf isotope characteristics of these high Sr/Y samples are also inconsistent with a magma mixing model. Consequently, the remaining scenario of partial melting of a thickened lower crust is discussed below.
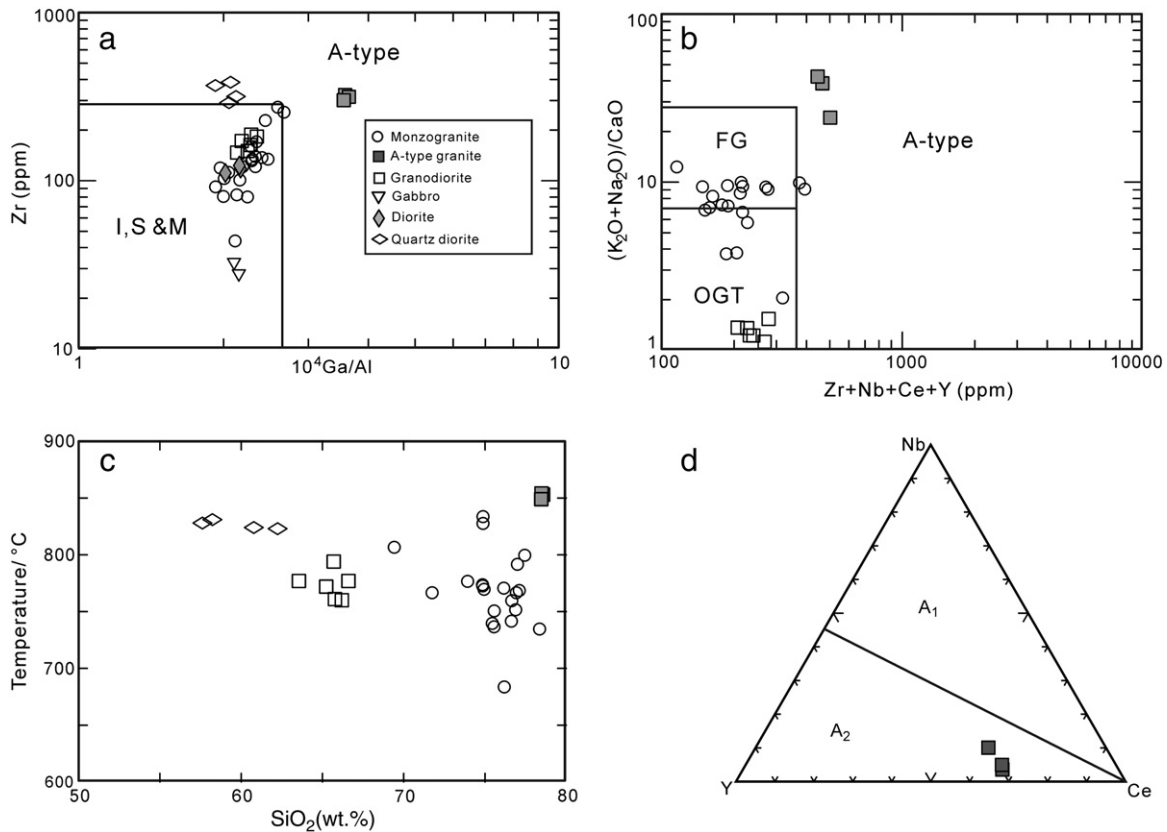
Partial melting of a thickened garnet-bearing mafic lower crust due to heat flux from the mantle (e.g., Atherton and Petford, 1993; Wang et al., 2005, 2007b) is a plausible mechanism for the generation of the high Sr/Y granodiorites. If the high Sr/Y magmas are actually derived from the mafic lower crust, then they should have relatively low MgO contents and be compositionally similar to 1–4.0 GPa experimental melts of metabasalts. In Fig. 4e, the samples display linear trends that are parallel to the fields of melts formed by partial melting of the thickened lower crust. This process is also consistent with the relatively low zircon $\delta^{18}O$ values (6.3–7.0‰) (Fig. 7a), which are within and slightly higher than the upper limit value of previously reported mantle-derived magma (6.5‰) (e.g., Valley et al., 2005). Additionally, the current crustal thickness of the Alxa Block is >45 km based on seismic data (Li, 2010).

6.2.2. Bijiertai Complex

The Bijiertai Complex contains many types of rocks, such as peridotites, gabbros, diorites, quartz diorites and newly discovered norites (Wang, 2012). However, the gabbros are cumulate rocks with REE patterns similar to other cumulate rocks (e.g., Ma et al., 2013a), thus, whole rock geochemical data cannot be used to constrain their sources. The low $\varepsilon_{Nd}(t)$ values (−9.9 to −9.5) of the gabbros, however, suggests that they were probably generated by partial melting of the lithospheric mantle.

The quartz diorites from the Bijiertai Complex have high Sr/Y ratios and the positive correlation between Sr/Y and Eu/Eu* (Fig. 9b) suggests that the plagioclase accumulation elevated the Sr/Y ratios (e.g., Ma et al., 2013b). The quartz diorites have $\varepsilon_{Nd}(t)$ values similar to the gabbros, indicating that they were probably generated by fractional crystallization from mafic magmas. Given that the quartz diorites have higher I_{Sr}, it is likely that they also assimilated small amounts of supracrustal materials.

The diorite $\varepsilon_{Nd}(t)$ value of −12.0 is lower than those of the gabbros and quartz diorites but similar to Bayannuoergong batholith granodiorites, indicating that they may have been generated by the partial melting of the crustal materials, although the involvement of mantle-derived materials cannot be excluded. The diorites have low Sr/Y ratios, suggesting that they were produced at mid-crustal depths. The diorites have zircon $\delta^{18}O$ values (6.80 ± 0.21‰) that are distinctly higher than those of Bayannuoergong batholith rocks derived by magma mixing (6.2–6.3‰) and slightly higher than those (6.61 ± 0.21‰) of the high Sr/Y granodiorites, consistent with a predominantly mid-crustal source.

Fig. 10. (a) Zr vs. 10^4Ga/Al and (b) (Na$_2$O + K$_2$O)/CaO vs. (Zr + Nb + Ce + Y) discrimination diagrams of Whalen et al. (1987), showing the A-type nature of a few granites; (c) temperature vs. SiO$_2$ for the Early Permian granitoids; (d) A$_1$ and A$_2$ subgroup discrimination of A-type granites after Eby (1992). I, S & M, unfractionated M-, I- and S-type granites (OGT); FG, fractionated felsic granites.

6.3. Geodynamics of the ca. 280 Ma magmatic flare-up

6.3.1. An extensional setting for the ca. 280 Ma magmatic rocks

The ~280 Ma granitoids were thought to have formed at an active continental margin based on geochemical discrimination diagrams (Li, 2006; Shi et al., 2012). However, these diagrams could instead reflect the tectonic settings in which the protoliths were formed, or reflect the melting of mixed sources (e.g., Li et al., 2003). The tectonic setting of the ~280 Ma granitoids can be constrained, however, by the timing of ocean closure between the CAOB and Alxa Block (i.e., Paleo-Asian Ocean), although this timing is itself highly disputed (e.g., Wang et al., 2010b; Wilhem et al., 2012; Xiao et al., 2009, 2010). Numerous Early Permian (ca. 280 Ma) A-type granites have been identified in the western CAOB (Tianshan, Junggar, and Altai) (Tang et al., 2010b; Zhang and Zou, 2013a and references therein) and are commonly attributed to the Permian Tarim mantle plume (e.g., Zhang and Zou, 2013a). This scenario implies that the Paleo-Asian Ocean was probably closed by this time. Recently, the Alxa Block has been invoked as a critical area to constrain the timing of Paleo-Asian Ocean closure, and subduction was proposed to extend into the Early Permian in the northern Alxa Block (Feng et al., 2013; Zhang et al., 2013b). However, this suggestion is not consistent with the spatial distribution and tectonic setting for the Upper Carboniferous–Lower Permian Amushan Formation. The Amushan Formation contains the only sedimentary stratum deposited in the Alxa Block during the Paleozoic. Moreover, the Amushan Formation occurs on both sides of the suture as adopted in this paper (Fig. 1b) but also to the north and south of the two sutures proposed by Feng et al. (2013). This distribution indicates that the tectonic setting of the northern Alxa Block had changed before the formation of the Amushan Formation. Indeed, the mafic rocks from the Amushan Formation were formed in a continental rifting setting (Dang et al., 2011; Jiang et al., 2011). Thus,

the ocean represented by the Enger Us Ophiolite must have been closed before the deposition of the Amushan Formation (Late Carboniferous–Early Permian).

Based on this evidence, the ca. 280 Ma magmatic rocks in the Alxa Block are likely to have been formed in a post-orogenic extensional setting. The proposed tectonic setting is also supported by the characteristics of the ca. 280 Ma magmatic rocks themselves. Although the I- and A-type granites and high Sr/Y rocks are very widespread globally, these three types of granitoids rarely occur synchronously together, except in a ridge subduction-related slab window (Tang et al., 2010a, 2012). However, the ca. 280 granitoids have evolved Sr–Nd isotopic compositions that are distinct from the depleted compositions found in their ridge subduction counterparts (Tang et al., 2010a, 2012). Moreover, no spatial or temporal zonation is apparent in the distribution of Alxa Block examples (Fig. 1b). Additionally, none of the magmatic rocks are significantly metamorphosed and no contemporaneous metamorphism occurred in the region. Thus, the ~280 Ma magmatic rocks must have formed in a post-collision extension or intraplate setting rather than in a ridge subduction environment.

6.3.2. An Early Permian mantle plume trigged the ca. 280 Ma magmatic flare-up?

The wide distribution and lack of zonation exhibited by the ca. 280 Ma Alxa Block magmatic rocks also argue against a slab break-off model (e.g., von Blanckenburg and Davis, 1995; Whalen et al., 2006, 2010). This model predicts a relatively narrow, linear zone of magmatism and uplift that is located along a suture zone. Two models could be proposed to account for intense post-collisional magmatism and the tectonic evolution, including (a) the detachment of an orogenic root zone or lithospheric delamination (e.g., Aydin et al., 2008; Whalen et al., 2006, 2010; Zhang et al., 2007), and (b) a mantle plume

(*e.g.*, Bryan et al., 2002; Li et al., 2003). Both processes may cause an up-welling of the asthenosphere and partial melting of various sources (Bonin, 2004), and yield similar magma evolution trends.

The model of lithospheric delamination seems feasible because of the distribution of ca. 280 granitoids in the Alxa Block (Fig. 1b). In this scenario, the post-collisional A-type granites occurred in lithospheric extensional regimes due to the upwelling of the asthenosphere caused by the lithospheric delamination (*e.g.*, Ilbeyli et al., 2004; Wu et al., 2002; Zhang et al., 2007). The association of coeval voluminous granites and minor mafic rocks in the Alxa Block is also similar to other proposed examples of lithospheric delamination, such as Mesozoic South China (*e.g.*, Li and Li, 2007), Mesozoic North China (*e.g.*, Wu et al., 2008) and the Late Paleozoic Iberia (*e.g.*, Gutiérrez-Alonso et al., 2011). However, these examples are accompanied by contemporaneous subduction systems, which did not exist in the Alxa Block and adjacent areas. More-over, the current lithospheric thickness of the Alxa Block is about 200 km (Zhang et al., 2012), reducing the plausibility of lithospheric delamination. The thick (~200 km) lithosphere and thick (>45 km) crust also reduces the plausibility of lithospheric extension as a mecha-nism for generating the ca. 280 Ma granitoids.

A mantle plume model does not share the weaknesses of the previ-ously described scenarios (*e.g.*, Bryan et al., 2002; Li et al., 2003). Early Permian igneous rocks are widely distributed in NW China (*e.g.*, Qin et al., 2011; Su et al., 2011; Xia et al., 2012; Xu et al., 2013; Zhang and Zou, 2013a, 2013b; Zhang et al., 2010), including the Tarim, Tianshan and CAOB, and constitute a large igneous province referred to as the Tarim or the Tianshan. A mantle plume has been invoked to explain the characteristics of these rocks (*e.g.*, Qin et al., 2011; Su et al., 2011; Xu et al., 2013; Zhang et al., 2010; Zhou et al., 2004), *e.g.*, widely distrib-uted basaltic rocks (*e.g.*, Zhang et al., 2010), extremely high magma tem-peratures estimated to be in the range of 1100–1600 °C (Qin et al., 2011), and widely distributed mafic–ultramafic complexes (*e.g.*, Qin et al., 2011). The Early Permian mantle plume was recently proposed to be situated closer to the Beishan Rift than the Eastern Tianshan and the western Tarim (Su et al., 2012). The ca. 280 Ma granitoids in the Alxa Block are coeval with the ca. 280 Ma Tarim mantle plume. Thus, the heat required to generate these crust-derived granitoids was likely supplied by the Tarim mantle plume given that the Alxa Block was probably near its margin. A similar example is the Chon Aike SLIP (188–153 Ma) (Pankhurst et al., 1998, 2000), which is adjacent to the Karoo–Ferrar LIP (Pankhurst et al., 2000).

Generating these large volume granitoids probably required the involvement of underplated mafic rocks in the lower crust, similar to other Phanerozoic SLIPs (*e.g.*, Bryan et al., 2002). The rare mafic rocks in the Alxa Block support the possibility of mafic underplating. More-over, the cumulus characteristics of the gabbro and quartz diorite imply the presence of magma chambers in the lower and upper crust. The main requirement for the generation of these large volume felsic melts is that their protoliths are hydrous (*e.g.*, Bryan et al., 2002), which is consistent with the fact that reported Phanerozoic SLIPs are all restricted to continental margins that acquire fertile, hydrous lower-crustal materials by long-lived subduction (*e.g.*, Bryan and Ferrari, 2013; Bryan et al., 2002). Although there is no contemporaneous subduction around the Alxa silicic igneous province, the hydrous lower-crust would have been created by Paleo-subduction in the southern (*e.g.*, Song et al., 2013), eastern (Dan et al., 2013) and northern (Zheng et al., 2013) part of the Alxa Block.

7. Conclusions

Most of the Phanerozoic igneous rocks in the Alxa Block were formed during a short period (290–250 Ma) with a magmatic flare-up at ca. 280 Ma and their large areal extent is similar to that of other silicic large igneous provinces. The A-type granite, I-type monzogranites and high Sr/Y granodiorites from the Bayannuoergong batholith were prob-ably generated by partial melting of underplated basalts, by the mixing

of lithospheric mantle-derived and lower crust-derived melts and by the remelting of the thickened lower crust, respectively. The gabbros, quartz diorites and diorites from the Bijiertai Complex were likely gen-erated by partial melting of the lithospheric mantle, differentiation from basaltic magmas and partial melting of the middle crust. The ca. 280 Ma magmatic event was probably formed in a post-orogenic extensional setting, and triggered by the adjacent ca. 280 Ma Tarim mantle plume.

Supplementary data to this article can be found online at http://dx.doi.org/10.1016/j.lithos.2014.01.018.

References

Allen, S.R., McPhie, J., Ferris, G., Simpson, C., 2008. Evolution and architecture of a large felsic igneous province in western Laurentia: the 1.6 Ga Gawler Range Volcanics, South Australia. Journal of Volcanology and Geothermal Research 172, 132–147.

Andersen, T., 2002. Correction of common lead in U–Pb analyses that do not report ^{204}Pb. Chemical Geology 192, 59–79.

Atherton, M.P., Petford, N., 1993. Generation of sodium-rich magmas from newly underplated basaltic crust. Nature 362, 144–146.

Aydin, F., Karsll, O., Chen, B., 2008. Petrogenesis of the Neogene alkaline volcanics with implications for post-collisional lithospheric thinning of the Eastern Pontides, NE Tur-key. Lithos 104, 249–266.

Belousova, E.A., Griffin, W.L., O'Reilly, S.Y., Fisher, N.I., 2002. Igneous zircon: trace element composition as an indicator of source rock type. Contributions to Mineralogy and Pe-trology 143, 602–622.

Betts, P.G., Giles, D., Foden, J., Schaefer, B.F., Mark, G., Pankhurst, M.J., Forbes, C.J., Williams, H.A., Chalmers, N.C., Hills, Q., 2009. Mesoproterozoic plume-modified orogenesis in eastern Precambrian Australia. Tectonics 28. http://dx.doi.org/10.1029/2008TC 002325 TC3006.

Bindeman, I.N., Eiler, J.M., Yogodzinski, G.M., Tatsumi, Y., Stern, C.R., Grove, T.L., Portnyagin, M., Hoernle, K., Danyushevsky, L.V., 2005. Oxygen isotope evidence for slab melting in modern and ancient subduction zones. Earth and Planetary Science Letters 235, 480–496.

Bonin, B., 2004. Do coeval mafic and felsic magmas in post-collisional to within-plate re-gimes necessarily imply two contrasting, mantle and crustal, sources? A review. Lith-os 78, 1–24.

Bryan, S., 2007. Silicic large igneous provinces. Episodes 30, 20–31.

Bryan, S.E., Ernst, R.E., 2008. Revised definition of large igneous provinces (LIPs). Earth-Science Reviews 86, 175–202.

Bryan, S.E., Ferrari, L., 2013. Large igneous provinces and silicic large igneous provinces: progress in our understanding over the last 25 years. Geological Society of America Bulletin 125, 1053–1078.

Bryan, S.E., Constantine, A.E., Stephens, C.J., Ewart, A., Schon, R.W., Parianos, J., 1997. Early Cretaceous volcano-sedimentary successions along the eastern Australian continental margin: implications for the break-up of eastern Gondwana. Earth and Planetary Sci-ence Letters 153, 85–102.

Bryan, S.E., Ewart, A., Stephens, C.J., Parianos, J., Downes, P.J., 2000. The Whitsunday Vol-canic Province, Central Queensland, Australia: lithological and stratigraphic investiga-tions of a silicic-dominated large igneous province. Journal of Volcanology and Geothermal Research 99, 55–78.

Bryan, S.E., Riley, T.R., Jerram, D.A., Stephens, C.J., Leat, P.T., 2002. Silicic volcanism: an undervalued component of large igneous provinces and volcanic rifted margins. In: Menzies, M.A., Klemperer, S.L., Ebinger, C.J., Baker, J. (Eds.), Volcanic Rifted Margins. Geological Society of America Special Paper, 362, pp. 97–118.

Bryan, S.E., Holcombe, R.J., Fielding, C.R., 2003. Yarrol terrane of the northern New En-gland Fold Belt: forearc or backarc? Reply. Australian Journal of Earth Sciences 50, 278–293.

Castillo, P.R., Janney, P.E., Solidum, R.U., 1999. Petrology and geochemistry of Camiguin Is-land, southern Philippines: insights to the source of adakites and other lavas in a complex arc setting. Contributions to Mineralogy and Petrology 134, 33–51.

Chen, Z.Y., Yang, S.S., Meng, E.G., Huang, Z.Q., 2004. Revision of Precambrian stratigraphic units in the Bayan Nuru area, Alxa Zuoqi, Inner Mongolia. Geological Bulletin of China 23, 345–351.

Chung, S.L., Jahn, B.M., Wu, G.Y., Lo, C.H., Cong, B.L., 1998. The Emeishan flood basalt in SW China: a mantle plume initiation model and its connection with continental breakup and mass extinction at the Permian–Triassic boundary. In: Flower, M.F.J., Chung, S.L., Lo, C.H., Lee, T.Y. (Eds.), Mantle Dynamics and Plate Interactions in East Asia, Geodynamics Series 27. American Geophysical Union, Washington, pp. 47–58.

Chung, S.L., Liu, D.Y., Ji, J.Q., Chu, M.F., Lee, H.Y., Wen, D.J., Lo, C.H., Lee, T.Y., Qian, Q., Zhang, Q., 2003. Adakites from continental collision zones: melting of thickened lower crust beneath southern Tibet. Geology 31, 1021–1024.

Coffin, M.F., Eldholm, O., 1994. Large igneous provinces: crustal structure, dimensions, and external consequences. Reviews of Geophysics 32, 1–36.

Collins, W.J., Beams, S.D., White, A.J.R., Chappell, B.W., 1982. Nature and origin of A-type granites with particular reference to Southeastern Australia. Contributions to Mineralogy and Petrology 80, 189–200.

Dan, W., Li, X.H., Guo, J.H., Liu, Y., Wang, X.C., 2012. Paleoproterozoic evolution of the eastern Alxa Block, westernmost North China: evidence from in situ zircon U–Pb dating and Hf–O isotopes. Gondwana Research 21, 838–864.

Dan, W., Li, X.H., Wang, Q., Wang, X.C., Liu, Y., 2013. Zircon U–Pb geochronology and Sr–Nd–Hf–O isotope geochemistry of the Paleozoic granitoids near eastern Alxa Block: petrogenesis and implications for the evolution of western North China Craton. Lithos (in revision).

Dan, W., Li, X.H., Wang, Q., Wang, X.C., Liu, Y., 2014. Neoproterozoic S-type granites in the Alxa Block, westernmost north China and tectonic implications: in-situ zircon U–Pb–Hf–O isotopic and geochemical constraints. American Journal of Science. http://dx.doi.org/10.2475/07.2013.00.

Dang, B., Zhao, H., Lin, G.C., Wu, K.L., Kang, X.Y., Ge, H.Y., Wu, B., Liu, S.H., 2011. Geochemistry and tectonic setting of Permian volcanic rocks in Yingen–Ejin Banner basin and its neighboring areas, western Inner Mongolia. Geological Bulletin of China 30, 923–931.

Defant, M.J., Drummond, M.S., 1990. Derivation of some modern arc magmas by melting of young subducted lithosphere. Nature 347, 662–665.

Defant, M.J., Xu, J.F., Kepezhinskas, P., Wang, Q., Zhang, Q., Xiao, L., 2002. Adakites: some variations on a theme. Acta Petrologica Sinica 18, 129–142.

Eby, G.N., 1990. The A-type granitoids: a review of their occurrence and chemical characteristics and speculations on their petrogenesis. Lithos 26, 115–134.

Eby, G.N., 1992. Chemical subdivision of the A-type granitoids: petrogenetic and tectonic implications. Geology 20, 641–644.

Ernst, R.E., Buchan, K.L., 2001. Large mafic magmatic events through time and links to mantle-plume heads. In: Ernst, R.E., Buchan, K.L. (Eds.), Mantle Plumes: Their Identification Through Time. Geological Society of America Special Paper, 352, pp. 483–575.

Ernst, R.E., Buchan, K.L., 2003. Recognizing mantle plumes in the geological record. Annual Review of Earth and Planetary Sciences 31, 469–523.

Feng, J.Y., Xiao, W.J., Windley, B., Han, C.M., Wan, B., Zhang, J.E., Ao, S.J., Zhang, Z.Y., Lin, L., 2013. Field geology, geochronology and geochemistry of mafic–ultramafic rocks from Alxa, China: implications for Late Permian accretionary tectonics in the southern Altaids. Journal of Asian Earth Sciences 78, 114–142.

Geng, Y.S., Zhou, X.W., 2012. Early Permian magmatic events in the Alxa metamorphic basement: evidence from geochronology. Acta Petrologica Sinica 28, 2667–2685.

Geng, Y.S., Wang, X.S., Shen, Q.H., Wu, C.M., 2002. The discovery of Neoproterozoic Jinningian deformed granites in Alxa area and its significance. Acta Petrologica et Mineralogica 21, 412–420.

Geng, Y.S., Wang, X.S., Shen, Q.H., Wu, C.M., 2007. Chronology of the Precambrian metamorphic series in the Alxa area, Inner Mongolia. Geology in China 34, 251–261.

Gong, J.H., Zhang, J.X., Yu, S.Y., 2011. The origin of Longshoushan Group and associated rocks in the southern part of the Alxa block: constraint from LA–ICP-MS U–Pb zircon dating. Acta Petrologica et Mineralogica 30, 795–818.

Gong, J.H., Zhang, J.X., Yu, S.Y., Li, H.K., Hao, K.J., 2012. The 2.5 Ga TTG in the western Alxa Block and its geological significance. Chinese Science Bulletin 57, 2715–2728.

Griffin, W.L., Pearson, N.J., Belousova, E.A., Saeed, A., 2006. Comment: Hf-isotope heterogeneity in zircon 91500. Chemical Geology 233, 358–363.

Guo, F., Nakamuru, E., Fan, W.M., Kobayoshi, K., Li, C.W., 2007. Generation of Palaeocene adakitic andesites by magma mixing; Yanji Area, NE China. Journal of Petrology 48, 661–692.

Gutiérrez-Alonso, G., Murphy, J.B., Fernandez-Suarez, J., Weil, A.B., Franco, M.P., Gonzalo, J.C., 2011. Lithospheric delamination in the core of Pangea: Sm–Nd insights from the Iberian mantle. Geology 39, 155–158.

Hu, Z.C., Liu, Y.S., Gao, S., Liu, W.G., Yang, L., Zhang, W., Tong, X.R., Lin, L., Zong, K.Q., Li, M., Chen, H.H., Zhou, L., Yang, L., 2012. Improved in situ Hf isotope ratio analysis of zircon using newly designed X skimmer cone and Jet sample cone in combination with the addition of nitrogen by laser ablation multiple collector ICP-MS. Journal of Analytical Atomic Spectrometry (JAAS) 27, 1391–1399.

Ilbeyli, N., Pearce, J.A., Thirlwall, M.F., Mitchell, J.G., 2004. Petrogenesis of collision-related plutonics in Central Anatolia, Turkey. Lithos 72, 163–182.

Jackson, S.E., Pearson, N.J., Griffin, W.L., Belousova, E.A., 2004. The application of laser ablation–inductively coupled plasma-mass spectrometry to in situ U–Pb zircon geochronology. Chemical Geology 211, 47–69.

Jiang, T., Li, Y.H., Chen, G.C., Wei, J.S., Li, J.C., 2011. Geochemical characteristics of Carboniferous–Permian Amushan Formation volcanic rocks in Ejin Banner and its vicinities, western Inner Mongolia. Geological Bulletin of China 30, 932–942.

Johnson, K., Barnes, C.G., Miller, C.A., 1997. Petrology, geochemistry, and genesis of high-Al tonalite and trondhjemites of the Cornucopia Stock, Blue Mountains, Northeastern Oregon. Journal of Petrology 38, 1585–1611.

Kay, S.M., Ramos, V.A., Marquez, M., 1993. Evidence in Cerro-Pampa volcanic-rocks for slab-melting prior to ridge–trench collision in southern South-America. The Journal of Geology 101, 703–714.

Kerr, A., Fryer, B.J., 1993. Nd isotope evidence for crust mantle interaction in the generation of A-type granitoid suites in Labrador, Canada. Chemical Geology 104, 39–60.

King, P.L., White, A.J.R., Chappell, B.W., Allen, C.M., 1997. Characterization and origin of aluminous A-type granites from the Lachlan Fold Belt, Southeastern Australia. Journal of Petrology 38, 371–391.

King, P.L., Chappell, B.W., Allen, C.M., White, A.J.R., 2001. Are A-type granites the high-temperature felsic granites? Evidence from fractionated granites of the Wangrah Suite. Australian Journal of Earth Sciences 48, 501–514.

Lai, X.R., Jiang, S.H., Qiu, X.P., Liu, Y., Hu, P., Zhang, W.Y., 2007. ^{40}Ar–^{39}Ar age and geochemical features of Hercynian intermediate acidity rock in Beidashan rock belt, Alxa. Acta Geologica Sinica 81, 370–380.

Li, J.J., 2006. Regional Metallogenic System of Alashan Block in Inner Mongolia Autonomous Region. China University of Geosciences, Beijing (Ph.D. thesis, 177p).

Li, T.D., 2010. The principal characteristics of the lithosphere of China. Geoscience Frontiers 1, 45–56.

Li, J., 2012. Characteristics and Tectonic Significance of Late Paleozoic Intrusive Rocks Along the Yabrai–Bayn Noel of Alxa, Inner Mongolia. China University of Geosciences, Beijing (Master thesis, 45p).

Li, Z.X., Li, X.H., 2007. Formation of the 1300-km-wide intracontinental orogen and postorogenic magmatic province in Mesozoic South China: a flat-slab subduction model. Geology 35, 179–182.

Li, X.H., Sun, M., Wei, G.J., Liu, Y., Lee, C.Y., Malpas, J., 2000. Geochemical and Sm–Nd isotopic study of amphibolites in the Cathaysia Block, southeastern China: evidence for an extremely depleted mantle in the Paleoproterozoic. Precambrian Research 102, 251–262.

Li, X.H., Li, Z.X., Ge, W.C., Zhou, H.W., Li, W.X., Liu, Y., Wingate, M.T.D., 2003. Neoproterozoic granitoids in South China: crustal melting above a mantle plume at ca. 825 Ma? Precambrian Research 122, 45–83.

Li, X.H., Liu, D.Y., Sun, M., Li, W.X., Liang, X.R., Liu, Y., 2004. Precise Sm–Nd and U–Pb isotopic dating of the supergiant Shizhuyuan polymetallic deposit and its host granite, SE China. Geological Magazine 141, 225–231.

Li, X.H., Qi, C.S., Liu, Y., Liang, X.R., Tu, X.L., Xie, L.W., Yang, Y.H., 2005. Petrogenesis of the Neoproterozoic bimodal volcanic rocks along the western margin of the Yangtze Block: new constraints from Hf isotopes and Fe/Mn ratios. Chinese Science Bulletin 50, 2481–2486.

Li, X.H., Liu, Y., Li, Q.L., Guo, C.H., Chamberlain, K.R., 2009. Precise determination of Phanerozoic zircon Pb/Pb age by multicollector SIMS without external standardization. Geochemistry, Geophysics, Geosystems 10. http://dx.doi.org/10.1029/2009GC002400 (Q04010).

Li, J.J., Zhai, Y.S., Yang, Y.Q., Wang, Y.B., Li, C.D., Cui, L.W., Zhou, H.Y., Liu, X.Y., Liu, X.X., Li, S., 2010a. Re-discussion on the metallogenic age of Zhulazaga gold deposit in Alashan Area, Inner Mongolia: evidence from zircon U–Pb SHRIMP age. Earth Science Frontiers 17, 178–184.

Li, J.J., Zhai, Y.S., Shang, H.Q., Li, H.M., Zhang, Y.S., Liu, S.Y., Wang, S.G., Sun, Z.P., Liu, X.X., 2010b. Metallogenic epoch of the Oubulage copper–gold deposit in the Alashan area, Inner Mongolia Autonomous Region. Bulletin of Mineralogy, Petrology and Geochemistry 29, 323–327.

Li, Q.L., Li, X.H., Liu, Y., Tang, G.Q., Yang, J.H., Zhu, W.G., 2010c. Precise U–Pb and Pb–Pb dating of Phanerozoic baddeleyite by SIMS with oxygen flooding technique. Journal of Analytical Atomic Spectrometry (JAAS) 25, 1107–1113.

Li, X.H., Li, W.X., Li, Q.L., Wang, X.C., Liu, Y., Yang, Y.H., 2010d. Petrogenesis and tectonic significance of the similar to 850 Ma Gangbian alkaline complex in South China: evidence from in situ zircon U–Pb dating, Hf–O isotopes and whole-rock geochemistry. Lithos 114, 1–15.

Li, X.H., Long, W.G., Li, Q.L., Liu, Y., Zheng, Y.F., Yang, Y.H., Chamberlain, K.R., Wan, D.F., Guo, C.H., Wang, X.C., Tao, H., 2010e. Penglai zircon megacrysts: a potential new working reference material for microbeam determination of Hf–O isotopes and U–Pb age. Geostandards and Geoanalytical Research 34, 117–134.

Li, Z.L., Chen, H.L., Song, B., Li, Y.Q., Yang, S.F., Yu, X., 2011. Temporal evolution of the Permian large igneous province in Tarim Basin, Northwest China. Journal of Asian Earth Sciences 42, 917–927.

Liu, S.A., Li, S.G., He, Y.S., Huang, F., 2010a. Geochemical contrasts between early Cretaceous ore-bearing and ore-barren high-Mg adakites in central-eastern China: implications for petrogenesis and Cu–Au mineralization. Geochimica et Cosmochimica Acta 74, 7160–7178.

Liu, Y.S., Gao, S., Hu, Z.C., Gao, C.G., Zong, K.Q., Wang, D.B., 2010b. Continental and oceanic crust recycling-induced melt–peridotite interactions in the Trans-North China Orogen: U–Pb dating, Hf isotopes and trace elements in zircons from mantle xenoliths. Journal of Petrology 51, 537–571.

Lu, J.C., Wei, X.Y., Li, Y.H., Wei, J.S., 2012. Geochemical characteristics of Carboniferous–Permian hydrocarbon source rocks of Xiangtan 9 well in Ejin Banner, western Inner Mongolia. Geological Bulletin of China 31, 1628–1638.

Ludwig, K.R., 2003. Users Manual for Isoplot 3.00: A Geochronological Toolkit for Microsoft Excel. Berkeley Geochronology Center, Special, Publication, 4.

Ma, L., Wang, Q., Li, Z.X., Wyman, D.A., Jiang, Z.Q., Yang, J.H., Gou, G.N., Guo, H.F., 2013a. Early Late Cretaceous (ca. 93 Ma) norites and hornblendites in the Milin area, eastern Gangdese: lithosphere–asthenosphere interaction during slab roll-back and an insight into early Late Cretaceous (ca. 100–80 Ma) magmatic "flare-up" in southern Lhasa (Tibet). Lithos 172–173, 17–30.

Ma, L., Wang, Q., Wyman, D.A., Jiang, Z.Q., Yang, J.H., Li, Q.L., Gou, G.N., Guo, H.F., 2013b. Late Cretaceous crustal growth in the Gangdese area, southern Tibet: petrological and Sr–Nd–Hf–O isotopic evidence from Zhengga diorite–gabbro. Chemical Geology 349–350, 54–70.

Macpherson, C.G., Dreher, S.T., Thirlwall, M.F., 2006. Adakites without slab melting: high pressure differentiation of island arc magma, Mindanao, the Philippines. Earth and Planetary Science Letters 243, 581–593.

Martin, H., Smithies, R.H., Rapp, R., Moyen, J.F., Champion, D., 2005. An overview of adakite, tonalite–trondhjemite–granodiorite (TTG), and sanukitoid: relationships and some implications for crustal evolution. Lithos 79, 1–24.

Middlemost, E.A.K., 1994. Naming materials in the magma/igneous rock system. Earth-Science Reviews 37, 215–224.

Mingram, B., Trumbull, R.B., Littman, S., Gerstenberger, H., 2000. A petrogenetic study of anorogenic felsic magmatism in the Cretaceous Paresis ring complex, Namibia: evidence for mixing of crust and mantle-derived components. Lithos 54, 1–22.

Moyen, J.F., 2009. High Sr/Y and La/Yb ratios: the meaning of the "adakitic signature". Lithos 112, 556–574.

Muir, R.J., Weaver, S.D., Bradshaw, J.D., Eby, G.N., Evans, J.A., 1995. The Cretaceous Separation Point batholith, New Zealand: granitoid magmas formed by melting of mafic lithosphere. Journal of the Geological Society of London 152, 689–701.

Mushkin, A., Navon, O., Halicz, L., Hartmann, G., Stein, M., 2003. The petrogenesis of A-type magmas from the Amram Massif, southern Israel. Journal of Petrology 44, 815–832.

NMBGMR(Nei Mongol Bureau of Geology and Mineral Resources), 1991. Regional Geology of Nei Mongol Autonomous Region. Geological Publishing House, Beijing 725 p.

Pankhurst, R.J., Leat, P.T., Sruoga, P., Rapela, C.W., Marquez, M., Storey, B.C., Riley, T.R., 1998. The Chon Aike province of Patagonia and related rocks in West Antarctica: a silicic large igneous province. Journal of Volcanology and Geothermal Research 81, 113–136.

Pankhurst, R.J., Riley, T.R., Fanning, C.M., Kelley, S.P., 2000. Episodic silicic volcanism in Patagonia and the Antarctic Peninsula: chronology of magmatism associated with the break-up of Gondwana. Journal of Petrology 41, 605–625.

Pankhurst, M.J., Schaefer, B.F., Betts, P.G., 2011a. Geodynamics of rapid voluminous felsic magmatism through time. Lithos 123, 92–101.

Pankhurst, M.J., Schaefer, B.F., Betts, P.G., Phillips, N., Hand, M., 2011b. A Mesoproterozoic continental flood rhyolite province, the Gawler Ranges, Australia: the end member example of the Large Igneous Province clan. Solid Earth 2, 25–33.

Petford, N., Atherton, M., 1996. Na-rich partial melts from newly underplated basaltic crust: the Cordillera Blanca batholith, Peru. Journal of Petrology 37, 1491–1521.

Pi, Q.H., Liu, C.Z., Chen, Y.L., Li, Y.Q., Li, D.P., 2010. Formation epoch and genesis of intrusive rocks in Huogeqi ore field of Inner Mongolia and their relationship with copper mineralization. Mineral Deposits 29, 437–451.

Qin, K.Z., Su, B.X., Sakyi, P.A., Tang, D.M., Li, X.H., Sun, H., Xiao, Q.H., Liu, P.P., 2011. SIMS zircon U–Pb geochronology and Sr–Nd isotopes of Ni–Cu-bearing mafic–ultramafic intrusions in Eastern Tianshan and Beishan in correlation with flood basalts in Tarim Basin (NW China): constraints on a ca. 280 Ma mantle plume. American Journal of Science 311, 237–260.

Ran, H., Zhang, W.J., Liu, Z.B., 2012. Geochemical characteristics and LA–ICP-MS zircon U–Pb dating of the Late Permian monzogranite in Hanggale, Alax Right Banner, Inner Mongolia. Geological Bulletin of China 31, 1565–1575.

Rapp, R.P., Watson, E.B., 1995. Dehydration melting of metabasalt at 8–32 kbar: implications for continental growth and crust–mantle recycling. Journal of Petrology 36, 891–931.

Rapp, R.P., Shimizu, N., Norman, M.D., Applegate, G.S., 1999. Reaction between slab-derived melts and peridotite in the mantle wedge: experimental constraints at 3.8 GPa. Chemical Geology 160, 335–356.

Richards, J.R., Kerrich, R., 2007. Special paper: adakite-like rocks: their diverse origins and questionable role in metallogenesis. Economic Geology 102, 537–576.

Rooney, T.O., Franceschi, P., Hall, C.M., 2011. Water-saturated magmas in the Panama Canal region: a precursor to adakite-like magma generation? Contributions to Mineralogy and Petrology 161, 373–388.

Sen, C., Dunn, T., 1994. Dehydration melting of a basaltic composition amphibolite at 1.5 and 2.0 GPa: implications for the origin of adakites. Contributions to Mineralogy and Petrology 117, 394–409.

Shi, X.J., Rong, Y., Wang, T., Zhang, J.J., Zhang, Z.C., Zhang, L., Guo, L., Zeng, T., Geng, J.Z., 2012. LA–ICP-MS zircon U–Pb age and geochemistry of the Early Permian Halinudeng granite in northern Alxa area, western Inner Mongolia. Geological Bulletin of China 31, 662–670.

Skjerlie, K.P., Patiño Douce, A.E., 2002. The fluid-absent partial melting of a zoisite bearing quartz eclogite from 1.0 to 3.2 GPa: implications for melting in thickened continental crust and for subduction-zone processes. Journal of Petrology 43, 291–314.

Sláma, J., Kosler, J., Condon, D.J., Crowley, J.L., Gerdes, A., Hanchar, J.M., Horstwood, M.S.A., Morris, G.A., Nasdala, L., Norberg, N., Schaltegger, U., Schoene, B., Tubrett, M.N., Whitehouse, M.J., 2008. Plešovice zircon—a new natural reference material for U–Pb and Hf isotopic microanalysis. Chemical Geology 249, 1–35.

Song, S.G., Niu, Y.L., Su, L., Xia, X.H., 2013. Tectonics of the North Qilian orogen, NW China. Gondwana Research 23, 1378–1401.

Springer, W., Seck, H.A., 1997. Partial fusion of basic granulites at 5 to 15 kbar: implications for the origin of TTG magmas. Contributions to Mineralogy and Petrology 127, 30–45.

Stern, C.R., Kilian, R., 1996. Role of the subducted slab, mantle wedge and continental crust in the generation of adakites from the Andean Austral volcanic zone. Contributions to Mineralogy and Petrology 123, 263–281.

Streck, M.J., Leeman, W.P., Chesley, J., 2007. High-magnesian andesite from Mount Shasta: a product of magma mixing and contamination, not a primitive mantle melt. Geology 35, 351–354.

Su, B.X., Qin, K.Z., Sakyi, P.A., Li, X.H., Yang, Y.H., Sun, H., Tang, D.M., Liu, P.P., Xiao, Q.H., Malaviarachchi, S.P.K., 2011. U–Pb ages and Hf–O isotopes of zircons from Late Paleozoic mafic–ultramafic units in southern Central Asian Orogenic Belt: tectonic implications and evidence for an Early-Permian mantle plume. Gondwana Research 20, 516–531.

Su, B.X., Qin, K.Z., Sun, H., Tang, D.M., Sakyi, P.A., Chu, Z.Y., Liu, P.-P., Xiao, Q.H., 2012. Subduction-induced mantle heterogeneity beneath Eastern Tianshan and Beishan:

insights from Nd–Sr–Hf–O isotopic mapping of Late Paleozoic mafic–ultramafic complexes. Lithos 134–135, 41–51.

Sun, S.S., McDonough, W.F., 1989. Chemical and isotopic systematics of oceanic basalt: implications for mantle composition and processes. In: Sanders, A.D., Norry, M.J. (Eds.), Magmatism in the Ocean Basins. Geological Society Special Publication, 42, pp. 528–548.

Sylvester, P.J., 1989. Post-collisional alkaline granites. The Journal of Geology 97, 261–280.

Tang, G.J., Wang, Q., Wyman, D.A., Li, Z.X., Zhao, Z.H., Jia, X.H., Jiang, Z.Q., 2010a. Ridge subduction and crustal growth in the Central Asian Orogenic Belt: evidence from Late Carboniferous adakites and high-Mg diorites in the western Junggar region, northern Xinjiang (west China). Chemical Geology 277, 281–300.

Tang, G.J., Wang, Q., Wyman, D.A., Sun, M., Li, Z.X., Zhao, Z.H., Sun, W.D., Jia, X.H., Jiang, Z.Q., 2010b. Geochronology and geochemistry of Late Paleozoic magmatic rocks in the Lamasu–Dabate area, northwestern Tianshan (west China): evidence for a tectonic transition from arc to post-collisional setting. Lithos 119, 393–411.

Tang, G.J., Wang, Q., Wyman, D.A., Li, Z.X., Zhao, Z.H., Yang, Y.H., 2012. Late Carboniferous high $\varepsilon_{Nd}(t)$–$\varepsilon_{Hf}(t)$ granitoids, enclaves and dikes in western Junggar, NW China: ridge-subduction-related magmatism and crustal growth. Lithos 140, 86–102.

Tung, K.A., Yang, H.Y., Liu, D.Y., Zhang, J.X., Tseng, C.Y., Wan, Y.S., 2007. SHRIMP U–Pb geochronology of the detrital zircons from the Longshoushan Group and its tectonic significance. Chinese Science Bulletin 52, 1414–1425.

Turner, S.P., Rushmer, T., 2009. Similarities between mantle-derived A-type granites and voluminous rhyolites in continental flood basalts provinces. Earth and Environmental Science Transactions of the Royal Society of Edinburgh 100, 1–10.

Turner, S.P., Foden, J.D., Morrison, R.S., 1992. Derivation of some A-type magmas by fractionation of basaltic magma; an example from the Padthaway Ridge, South Australia. Lithos 28, 151–179.

Valley, J.W., 2003. Oxygen isotopes in zircon. Review in Mineralogy and Geochemistry 53, 343–385.

Valley, J.W., Lackey, J.S., Cavosie, A.J., Clechenko, C.C., Spicuzza, M.J., Basei, M.A.S., Bindeman, I.N., Ferreira, V.P., Sial, A.N., King, E.M., Peck, W.H., Sinha, A.K., Wei, C.S., 2005. 4.4 billion years of crustal maturation: oxygen isotope ratios of magmatic zircon. Contributions to Mineralogy and Petrology 150, 561–580.

von Blanckenburg, F., Davis, J.H., 1995. Slab breakoff: a model for syncollisional magmatism and tectonics in the Alps. Tectonics 14, 120–131.

Wang, X.J., 2012. The Geochemical Characters and its Tectonic Implications of Ophiolites in Alxa Area, Inner Mongolia. China University of Geosciences, Beijing (Ph.D. thesis, 208p).

Wang, Q., McDermott, F., Xu, J.F., Bellon, H., Zhu, Y.T., 2005. Cenozoic K-rich adakitic volcanic rocks in the Hohxil area, northern Tibet: lower-crustal melting in an intracontinental setting. Geology 33, 465–468.

Wang, Q., Xu, J.F., Jian, P., Bao, Z.W., Zhao, Z.H., Li, C.F., Xiong, X.L., Ma, J.L., 2006. Petrogenesis of adakitic porphyries in an extensional tectonic setting, Dexing, South China: implications for the genesis of porphyry copper mineralization. Journal of Petrology 47, 119–144.

Wang, Q., Wyman, D., Zhao, Z., Xu, J., Bai, Z., Xiong, X., Dai, T., Li, C., Chu, Z., 2007a. Petrogenesis of Carboniferous adakites and Nb-enriched arc basalts in the Alataw area, northern Tianshan Range (western China): implications for Phanerozoic crustal growth in the Central Asia orogenic belt. Chemical Geology 236, 42–64.

Wang, Q., Wyman, D.A., Xu, J.F., Jian, P., Zhao, Z.H., Li, C.F., Xu, W., Ma, J.L., He, B., 2007b. Early Cretaceous adakitic granites in the Northern Dabie Complex, central China: implications for partial melting and delamination of thickened lower crust. Geochimica et Cosmochimica Acta 71, 2609–2636.

Wang, Q., Wyman, D.A., Xu, J.F., Wan, Y.S., Li, C.F., Zi, F., Jiang, Z.Q., Qiu, H.N., Chu, Z.Y., Zhao, Z.H., Dong, Y.H., 2008. Triassic Nb-enriched basalts, magnesian andesites, and adakites of the Qiangtang terrane (Central Tibet): evidence for metasomatism by slab-derived melts in the mantle wedge. Contributions to Mineralogy and Petrology 155, 473–490.

Wang, Q., Wyman, D.A., Li, Z.X., Bao, Z.W., Zhao, Z.H., Wang, Y.X., Jian, P., Yang, Y.H., Chen, L.L., 2010a. Petrology, geochronology and geochemistry of ca. 780 Ma A-type granites in South China: petrogenesis and implications for crustal growth during the breakup of the supercontinent Rodinia. Precambrian Research 178, 185–208.

Wang, Q.C., Shu, L.S., Charvet, J., Faure, M., Ma, H.D., Natal'in, B., Gao, J., Kroner, A., Xiao, W.J., Li, J.Y., Windley, B., Chen, Y., Glen, R., Jian, P., Zhang, W., Seltmann, R., Wilde, S., Choulet, F., Wan, B., Quinn, C., Rojas-Agramonte, Y., Shang, Q.H., Zhang, W., Wang, B., Lin, W., 2010b. Understanding and study perspectives on tectonic evolution and crustal structure of the Paleozoic Chinese Tianshan. Episodes 33, 242–266.

Wei, X., Xu, Y.G., Feng, Y.X., Zhao, J.X., 2014. Lithosphere–mantle plume interaction in the formation of Tarim Large Igneous Province: geochronological and geochemical constraints. American Journal of Science 314. http://dx.doi.org/10.2475/04.2014.00.

Whalen, J.B., Currie, K.L., Chappell, B.W., 1987. A-type granites: geochemical characteristics, discrimination and petrogenesis. Contributions to Mineralogy and Petrology 95, 407–419.

Whalen, J.B., McNicoll, V.J., van Staal, C.R., Lissenberg, C.J., Longstaffe, F.J., Jenner, G.A., van Breeman, O., 2006. Spatial, temporal and geochemical characteristics of Silurian collision-zone magmatism, Newfoundland Appalachians: an example of a rapidly evolving magmatic system related to slab break-off. Lithos 89, 377–404.

Whalen, J.B., Wodicka, N., Taylor, B.E., Jackson, G.D., 2010. Cumberland batholith, Trans-Hudson Orogen, Canada: petrogenesis and implications for Paleoproterozoic crustal and orogenic processes. Lithos 117, 99–118.

Wiedenbeck, M., Alle, P., Corfu, F., Griffin, W.L., Meier, M., Oberli, F., Vonquadt, A., Roddick, J.C., Speigel, W., 1995. 3 natural zircon standards for U–Th–Pb, Lu–Hf, trace-element and REE analyses. Geostandards Newsletter 19, 1–23.

Wiedenbeck, M., Hanchar, J.M., Peck, W.H., Sylvester, P., Valley, J., Whitehouse, M., Kronz, A., Morishita, Y., Nasdala, L., Fiebig, J., Franchi, I., Girard, J.P., Greenwood, R.C., Hinton, R., Kita, N., Mason, P.R.D., Norman, M., Ogasawara, M., Piccoli, R., Rhede, D., Satoh, H.,

Schulz-Dobrick, B., Skar, O., Spicuzza, M.J., Terada, K., Tindle, A., Togashi, S., Vennemann, T., Xie, Q., Zheng, Y.F., 2004. Further characterisation of the 91500 zircon crystal. Geostandards and Geoanalystical Research 28, 9–39.

Wilhem, C., Windley, B.F., Stampfli, G.M., 2012. The Altaids of Central Asia: a tectonic and evolutionary innovative review. Earth-Science Reviews 113, 303–341.

Wu, K.L., 2011. Geochemical Characteristics and Tectonic Setting of Late Varisian Period in Alashan Block. Chang'an University Xi'an (Master thesis, 70p).

Wu, F.Y., Sun, D.Y., Li, H.M., Jahn, B.M., Wilde, S., 2002. A-type granites in northeastern China: age and geochemical constraints on their petrogenesis. Chemical Geology 187, 143–173.

Wu, F.Y., Yang, Y.H., Xie, L.W., Yang, J.H., Xu, P., 2006. Hf isotopic compositions of the standard zircons and baddeleyites used in U–Pb geochronology. Chemical Geology 234, 105–126.

Wu, F.Y., Xu, Y.G., Gao, S., Zheng, J.P., 2008. Lithospheric thinning and destruction of the North China Craton. Acta Petrologica Sinica 24, 1145–1174.

Xia, L.Q., Xu, X.Y., Li, X.M., Ma, Z.P., Xia, Z.C., 2012. Reassessment of petrogenesis of Carboniferous–Early Permian rift-related volcanic rocks in the Chinese Tianshan and its neighboring areas. Geoscience Frontiers 3, 445–471.

Xiao, W.J., Windley, B.F., Yuan, C., Sun, M., Han, C.M., Lin, S.F., Chen, H.L., Yan, Q.R., Liu, D.Y., Qin, K.Z., Li, J.L., Sun, S., 2009. Paleozoic multiple subduction–accretion processes of the Southern Altaids. American Journal of Science 309, 221–270.

Xiao, W.J., Mao, Q.G., Windley, B.F., Han, C.M., Qu, J.F., Zhang, J.E., Ao, S.J., Guo, Q.Q., Cleven, N.R., Lin, S.F., Shan, Y.H., Li, J.L., 2010. Paleozoic multiple accretionary and collisional processes of the Beishan orogenic collage. American Journal of Science 310, 1553–1594.

Xie, L.W., Zhang, Y.B., Zhang, H.H., Sun, J.F., Wu, F.Y., 2008. *In situ* simultaneous determination of trace elements, U–Pb and Lu–Hf isotopes in zircon and baddeleyite. Chinese Science Bulletin 53, 1565–1573.

Xu, Y.G., He, B., Luo, Z.Y., Liu, H.Q., 2013. Large igneous provinces in China and mantle plume: an overview and perspectives. Bulletin of Mineralogy, Petrology and Geochemistry 32, 25–39.

Yang, J.H., Wu, F.Y., Chung, S.L., Wilde, S.A., Chu, M.F., 2006. A hybrid origin for the Qianshan A-type granite, northeast China: geochemical and Sr–Nd–Hf isotopic evidence. Lithos 89, 89–106.

Yang, S.F., Li, Z.L., Chen, H.L., Santosh, M., Dong, C.W., Yu, X., 2007. Permian bimodal dyke of Tarim Basin, NW China: geochemical characteristics and tectonic implications. Gondwana Research 12, 113–120.

Yang, S.F., Chen, H.L., Li, Z.L., Li, Y.Q., Yu, X., Li, D.X., Meng, L.F., 2013. Early Permian Tarim Large Igneous Province in northwest China. Science China Earth Sciences 56, 2015–2026.

Zeh, A., Gerdes, A., Klemd, R., Barton, J.M., 2007. Archaean to Proterozoic crustal evolution in the Central Zone of the Limpopo Belt (South Africa–Botswana): constraints from combined U–Pb and Lu–Hf isotope analyses of zircon. Journal of Petrology 48, 1605–1639.

Zhang, C.L., Zou, H.B., 2013a. Permian A-type granites in Tarim and western part of Central Asian Orogenic Belt (CAOB): genetically related to a common Permian mantle plume? Lithos 172–173, 47–60.

Zhang, C.L., Zou, H.b., 2013b. Comparison between the Permian mafic dykes in Tarim and the western part of Central Asian Orogenic Belt (CAOB), NW China: implications for two mantle domains of the Permian Tarim Large Igneous Province. Lithos 174, 15–27.

Zhang, H.F., Parrish, R., Zhang, L., Xu, W.C., Yuan, H.L., Gao, S., Crowley, Q.G., 2007. A-type granite and adakitic magmatism association in Songpan–Garze fold belt, eastern Tibetan Plateau: implication for lithospheric delamination. Lithos 97, 323–335.

Zhang, C.L., Li, Z.X., Li, X.H., Xu, Y.G., Zhou, G., Ye, H.M., 2010. A Permian large igneous province in Tarim and Central Asian orogenic belt, NW China: results of a ca. 275 Ma mantle plume? Geological Society of America Bulletin 122, 2020–2040.

Zhang, H.S., Teng, J.W., Tian, X.B., Zhang, Z.J., Gao, R., Liu, J.Q., 2012. Lithospheric thickness and upper-mantle deformation beneath the NE Tibetan Plateau inferred from S receiver functions and SKS splitting measurements. Geophysical Journal International 191, 1285–1294.

Zhang, J.X., Gong, J.H., Yu, S.Y., Li, H.K., Hou, K.J., 2013a. Neoarchean–Paleoproterozoic multiple tectonothermal events in the western Alxa block, North China Craton and their geological implication: evidence from zircon U–Pb ages and Hf isotopic composition. Precambrian Research 235, 36–57.

Zhang, W., Wu, T.R., Feng, J.C., Zheng, R.G., He, Y.K., 2013b. Time constraints for the closing of the Paleo-Asian Ocean in the Northern Alxa Region: evidence from Wuliji granites. Science China Earth Sciences 56, 153–164.

Zhao, G.C., Sun, M., Wilde, S.A., Li, S.Z., 2005. Late Archean to Paleoproterozoic evolution of the North China Craton: key issues revisited. Precambrian Research 136, 177–202.

Zheng, R., Wu, T., Zhang, W., Xu, C., Meng, Q., Zhang, Z., 2013. Late Paleozoic subduction system in the northern margin of the Alxa block, Altaids: geochronological and geochemical evidence from ophiolites. Gondwana Research. http://dx.doi.org/10.1016/j.gr.2013.05.011.

Zhou, M.F., Lesher, C.M., Yang, Z.X., Li, J.W., Sun, M., 2004. Geochemistry and petrogenesis of 270 Ma Ni–Cu–(PGE) sulfide-bearing mafic intrusions in the Huangshan district, eastern Xinjiang, northwest China: implications for the tectonic evolution of the Central Asian orogenic belt. Chemical Geology 209, 233–257.

Zhou, M.F., Zhao, J.H., Jiang, C.Y., Gao, J.F., Wang, W., Yang, S.H., 2009. OIB-like, heterogeneous mantle sources of Permian basaltic magmatism in the western Tarim Basin, NW China: implications for a possible Permian large igneous province. Lithos 113, 583–594.

Zindler, A., Hart, S., 1986. Chemical geodynamics. Annual Review of Earth and Planetary Sciences 14, 493–571.